

Thermal versus entropic Mpemba effect in molecular gases with nonlinear drag

Alberto Megías*

Departamento de Física, Universidad de Extremadura, E-06006 Badajoz, Spain

Andrés Santos†

*Departamento de Física, Universidad de Extremadura, E-06006 Badajoz, Spain and
Instituto de Computación Científica Avanzada (ICCAEx),
Universidad de Extremadura, E-06006 Badajoz, Spain*

Antonio Prados‡

Física Teórica, Universidad de Sevilla, Apartado de Correos 1065, E-41080 Sevilla, Spain

(Dated: May 31, 2022)

Loosely speaking, the Mpemba effect appears when hotter systems cool sooner or, in a more abstract way, when systems further from equilibrium relax faster. In this paper, we investigate the Mpemba effect in a molecular gas with nonlinear drag, both analytically (by employing the tools of kinetic theory) and numerically (direct simulation Monte Carlo of the kinetic equation and event-driven molecular dynamics). The analysis is carried out via two alternative routes, recently considered in the literature: first, the kinetic or thermal route, in which the Mpemba effect is characterized by the crossing of the evolution curves of the kinetic temperature (average kinetic energy), and, second, the stochastic thermodynamics or entropic route, in which the Mpemba effect is characterized by the crossing of the distance to equilibrium in probability space. In general, a nonmutual correspondence between the thermal and entropic Mpemba effects is found, i.e., there may appear the thermal effect without its entropic counterpart or vice versa. Furthermore, a nontrivial overshoot with respect to equilibrium of the thermal relaxation makes it necessary to revise the usual definition of the thermal Mpemba effect, which is shown to be better described in terms of the relaxation of the local equilibrium distribution. Our theoretical framework, which involves an extended Sonine approximation in which not only the excess kurtosis but also the sixth cumulant is retained, gives an excellent account of the behavior observed in simulations.

I. INTRODUCTION

In recent years, memory effects have become a hot topic in nonequilibrium statistical physics research [1]. Those phenomena usually imply counterintuitive effects that apparently contradict well-established standard physical laws. One of the most interesting is the Mpemba effect (ME): Given two samples of a fluid in a common thermal bath, the initially hotter one may cool more rapidly than that initially cooler. The well-known Newton’s law of cooling, according to which the temperature evolution is predetermined by its initial value, is thus violated in the presence of the ME. Original studies of the ME deal with water [2–32], and even today there is still a lack of consensus about its existence in this very complex system [33–35].

In a more general context, the ME can be recast as “the initially further from equilibrium relaxes faster,” with the separation from equilibrium being defined in a suitable way, see below. With such an interpretation, Mpemba-like effects have been investigated in a large variety of many-body systems: molecular gases [36, 37], mixtures [38], granular gases [39–45], inertial suspen-

sions [46, 47], spin glasses [48], carbon nanotube resonators [49], clathrate hydrates [50], Markovian models [51–55], active systems [56], Ising models [57–59], non-Markovian mean-field systems [60, 61], or quantum systems [62]. Very recently, the ME has been analyzed in the framework of Landau’s theory of phase transitions [63]. Also, it has been experimentally observed in colloids [64, 65].

There have been two main approaches to the ME: the kinetic-theory or “thermal” approach [36–44, 46, 47] and the stochastic-process (or thermodynamics) or “entropic” approach [51–56, 62, 64, 65]. In the thermal approach, kinetic theory makes it possible to define in a natural way an out-of-equilibrium time-dependent temperature $T(t)$ as basically the average kinetic energy, i.e.,

$$T(t) = \frac{m}{dk_B} \langle v^2 \rangle, \quad (1)$$

where d is the dimensionality of the system, m is the mass of a particle, and k_B is the Boltzmann constant. This definition allows for a simple, and close in spirit to the original studies in water, characterization of the separation from equilibrium at temperature T_{eq} : The initially hotter (colder) sample A (B) translates into that having the larger (smaller) initial value of the kinetic temperature, $T_A^0 > T_B^0 > T_{\text{eq}}$. A *thermal* Mpemba effect (TME) is observed if the evolution curves for the temperature cross at a certain time t_θ , $T_A(t_\theta) = T_B(t_\theta)$, and that of the initially hotter remains below the other one for longer

* albertom@unex.es

† andres@unex.es

‡ prados@us.es

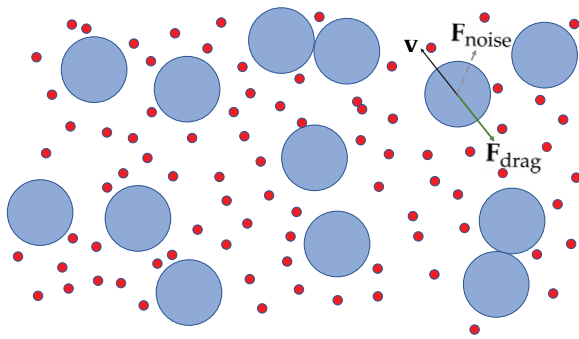


FIG. 1. Illustration of the system considered in this paper. A molecular gas of hard particles (represented by the large blue circles) is coupled to a thermal bath (made of particles represented by the small red circles) via a drag force $\mathbf{F}_{\text{drag}} = -m\zeta(v)\mathbf{v}$, where $\zeta(v)$ is a velocity-dependent drag coefficient, and a stochastic force $\mathbf{F}_{\text{noise}} = m\xi(v)\boldsymbol{\eta}$, where $\boldsymbol{\eta}$ is a Gaussian white-noise term. In addition, the particles are subjected to binary elastic collisions.

times, $T_{\text{eq}} < T_A(t) < T_B(t)$ for $t > t_\theta$. Additionally, a Mpemba effect may exist in the absence of a temperature crossing if $T_B(t)$ overshoots the equilibrium value at a certain time t_O , i.e., $T_B(t_O) = T_{\text{eq}}$, then reaches a minimum, and finally relaxes to equilibrium later than sample A. This overshoot effect would be the analog of the supercooling phenomenon in water.

In the stochastic-process approach, the starting point is usually a Markov process $\mathbf{x}(t)$. The state of the system at time t is determined by a probability distribution $P(\mathbf{x}, t)$, which typically obeys a master equation, for discrete \mathbf{x} , or a Fokker–Planck equation, for continuous \mathbf{x} . The Kullback–Leibler divergence (KLD) or relative entropy [66] is defined as

$$\mathcal{D}(t) \equiv \left\langle \ln \frac{P}{P^{\text{eq}}} \right\rangle = \int d\mathbf{x} P(\mathbf{x}, t) \ln \frac{P(\mathbf{x}, t)}{P^{\text{eq}}(\mathbf{x})}, \quad (2)$$

where $P^{\text{eq}}(\mathbf{x})$ stands for the equilibrium probability distribution. The H -theorem [67] ensures that $\mathcal{D}(t)$ monotonically decreases to zero over a nonequilibrium process and thus $\mathcal{D}(t)$ can be interpreted as the distance to equilibrium from a physical standpoint [68]. Also, \mathcal{D} can be understood as (the opposite of) the nonequilibrium entropy relative to the equilibrium state. The ME is translated as follows in this context: The further from (closer to) sample A (B) has the larger (smaller) initial value of \mathcal{D} , i.e., $\mathcal{D}_A^0 > \mathcal{D}_B^0 > 0$. The entropic Mpemba effect (EME) emerges when the evolution curves for \mathcal{D} cross at a certain time $t_{\mathcal{D}}$, $\mathcal{D}_A(t_{\mathcal{D}}) = \mathcal{D}_B(t_{\mathcal{D}})$, and $0 < \mathcal{D}_A(t) < \mathcal{D}_B(t)$ for $t > t_{\mathcal{D}}$.

The two effects described above, TME and EME, are equivalent if a biunivocal correspondence between nonequilibrium temperature and (entropic) distance to equilibrium exists. Yet, this is not the case in general, as we will show. In fact, the main aim of this paper is to analyze the correspondence between the TME and

the EME in a prototypical system, where the two approaches can be carried out analytically—at least in an approximate, systematic, way. Specifically, we consider a molecular gas of hard particles that is coupled to a thermal bath, with the resulting drag force being nonlinear in the velocity [36]. In addition, there are binary elastic collisions between the particles. See Fig. 1 for an illustration of the system. The evolution equation of the velocity distribution function (VDF) is given by the Enskog–Fokker–Planck equation (EFPE)—the Enskog term accounts for binary collisions, whereas the Fokker–Planck term models the interaction with the thermal bath, see Sec. II for details. To look into the system dynamics, we employ a hybrid approach that includes both a theoretical and a numerical analysis: kinetic-theory tools—via a Sonine approximation of the EFPE equation—for the former and direct simulation Monte Carlo (DSMC), together with event-driven molecular dynamics (EDMD), simulations for the latter.

Note that it is the nonlinearity of the drag force that the ME stems from. As a consequence, the time evolution of the kinetic temperature is coupled to other moments and the kinetic temperature of the nonlinear fluid shows algebraic nonexponential relaxation and strong memory effects after a quench [37]. Note also that elastic collisions do not change the average kinetic energy: Were the drag absent, the kinetic temperature would remain constant throughout the whole time evolution. Still, an initial nonequilibrium VDF would evolve toward the equilibrium Maxwellian—higher-order velocity cumulants would indeed be affected by collisions and tend to zero in the long-time limit.

The above characterizations of out-of-equilibrium temperature and distance to equilibrium, Eqs. (1) and (2), are quite natural in the molecular fluid. Yet, a different choice may be more adequate in other systems. On the one hand, some kind of nonequilibrium temperature, e.g., in the spirit of the fictive or effective temperature for glassy systems [69–71], may be introduced in systems where the kinetic temperature cannot be defined—for example, Ising models [72]. On the other hand, the L_1 and L_2 norms have been employed in the literature to measure the distance of the VDF to equilibrium [51, 54, 64]. Alternative choices for the observables characterizing the thermal relaxation and the distance to equilibrium may quantitatively affect the values of the crossing times t_θ and $t_{\mathcal{D}}$, and even the own existence of the TME and the EME.

With the above definitions, both the TME and the EME can be investigated. Some basic questions arise, though. Does the TME imply the EME, or vice versa? When both of them are present, how close are the respective crossover times t_θ and $t_{\mathcal{D}}$? Is it possible to observe the ME if the kinetic temperature of at least one of the two samples overshoots its equilibrium value? The theoretical framework developed in this paper, which is supported by computer simulations, answers these key questions.

The paper is organized as follows. Section II puts forward our model system for a fluid with nonlinear drag. Also, the local equilibrium concept is introduced and its implications for the entropic distance are discussed. In Sec. III, we derive the evolution equations for the relevant physical quantities, within the Sonine approximation schemes developed in this paper. From this knowledge, the general phenomenology of TME and EME is predicted and described from heuristic arguments in Sec. IV. Afterwards, in Sec. V a singular case for TME, induced by the appearance of an overshoot effect, is investigated. Thus, Secs. II–V constitute the core of the theoretical framework developed in the paper. In addition, we present simulation results supporting the theoretical predictions in Sec. VI. Finally, conclusions are presented in Sec. VII, including a discussion on the definition of nonequilibrium temperature for a general system. Some technical parts are relegated to appendices.

II. MODEL SYSTEM AND LOCAL EQUILIBRIUM

Let us consider the following model for a fluid with nonlinear drag [36, 37, 73–75]: a d -dimensional fluid of elastic hard spheres of mass m and diameter σ , with number density n , subjected to a stochastic force composed by a white-noise term with nonlinear variance plus a nonlinear drag force. This scheme mimics a system of elastic spheres assumed to be suspended in a background fluid in equilibrium at temperature T_b , as depicted in Fig. 1.

The (spatially uniform) EFPE for the one-body VDF $f(\mathbf{v}, t)$ reads

$$\partial_t f(\mathbf{v}, t) - \frac{\partial}{\partial \mathbf{v}} \cdot \left[\zeta(v) \mathbf{v} + \frac{\xi^2(v)}{2} \frac{\partial}{\partial \mathbf{v}} \right] f(\mathbf{v}, t) = J[\mathbf{v}|f, f], \quad (3)$$

where

$$J[\mathbf{v}_1|f, f] = \sigma^{d-1} g_c \int d\mathbf{v}_2 \int_+ d\hat{\boldsymbol{\sigma}} \mathbf{v}_{12} \cdot \hat{\boldsymbol{\sigma}} \times [f(\mathbf{v}'_1, t) f(\mathbf{v}'_2, t) - f(\mathbf{v}_1, t) f(\mathbf{v}_2, t)] \quad (4)$$

is the usual Boltzmann–Enskog collision operator with $\mathbf{v}_{12} \equiv \mathbf{v}_1 - \mathbf{v}_2$, $g_c = \lim_{r \rightarrow \sigma^+} g(r)$ being the contact value of the pair correlation function, and $\int_+ d\hat{\boldsymbol{\sigma}} \equiv \int d\hat{\boldsymbol{\sigma}} \Theta(\mathbf{v}_{12} \cdot \hat{\boldsymbol{\sigma}})$. In addition, the drag component of the stochastic force is $-m\zeta(v)\mathbf{v}$, while the white-noise counterpart has a nonlinear variance $m^2\xi^2(v)$. The functions $\zeta(v)$ and $\xi^2(v)$ are connected via the fluctuation-dissipation theorem as

$$\xi^2(v) = \frac{2k_B T_b}{m} \zeta(v), \quad (5)$$

where T_b is the temperature of the background fluid. This ensures that the only stationary solution of the EFPE is the equilibrium Maxwellian,

$$f^{\text{eq}}(\mathbf{v}) = n \left(\frac{m}{2\pi k_B T_b} \right)^{d/2} e^{-mv^2/2k_B T_b}. \quad (6)$$

A quadratic dependence of the drag coefficient naturally appears when the hard spheres and the background fluid particles have a comparable mass [36, 37, 73–75],

$$\zeta(v) = \zeta_0 \left(1 + \gamma \frac{mv^2}{k_B T_b} \right). \quad (7)$$

The coefficients ζ_0 and γ are both positive and measure the zero-velocity value of the drag coefficient and the degree of nonlinearity of the drag force, respectively. Note that, due to the nonlinearity of the drag force, the implementation of the Langevin equation associated with the free streaming of particles between collisions is far from trivial. This issue is discussed in Appendix A.

The two approaches to the ME can be implemented in the nonlinear fluid introduced above. Translating Eqs. (1) and (2) to our model system, we have that the nonequilibrium temperature $T(t)$ is given by

$$T(t) = \frac{m}{dk_B} \langle v^2 \rangle = \frac{m}{ndk_B} \int d\mathbf{v} v^2 f(\mathbf{v}, t), \quad (8)$$

and the relative entropy is

$$\mathcal{D}(t) = \left\langle \ln \frac{f}{f^{\text{eq}}} \right\rangle = \frac{1}{n} \int d\mathbf{v} f(\mathbf{v}, t) \ln \frac{f(\mathbf{v}, t)}{f^{\text{eq}}(\mathbf{v})}, \quad (9)$$

where $n \equiv \int d\mathbf{v} f(\mathbf{v}, t)$ is the number density.

On physical grounds, it is expected that the evolution of the gas toward equilibrium takes place along two stages [76]. First, a rapid “kinetic” stage where the VDF approaches the so-called local equilibrium (LE) form,

$$f^{\text{LE}}(\mathbf{v}; T(t)) = n \left[\frac{m}{2\pi k_B T(t)} \right]^{d/2} e^{-mv^2/2k_B T(t)}, \quad (10)$$

i.e., f^{LE} has the Maxwellian shape but with the time-dependent temperature. Second, a slower “hydrodynamic” stage, where the VDF is close to f^{LE} and the evolution of the VDF takes place via the temperature.

The above discussion suggests the following decomposition for the relative entropy,

$$\mathcal{D}(t) = \mathcal{D}^{\text{kin}}(t) + \mathcal{D}^{\text{LE}}(T(t)), \quad (11)$$

where

$$\mathcal{D}^{\text{kin}}(t) = \frac{1}{n} \int d\mathbf{v} f(\mathbf{v}, t) \ln \frac{f(\mathbf{v}, t)}{f^{\text{LE}}(\mathbf{v}; T(t))} \quad (12a)$$

and

$$\begin{aligned} \mathcal{D}^{\text{LE}}(T(t)) &= \frac{1}{n} \int d\mathbf{v} f^{\text{LE}}(\mathbf{v}; T(t)) \ln \frac{f^{\text{LE}}(\mathbf{v}; T(t))}{f^{\text{eq}}(\mathbf{v})} \\ &= \frac{d}{2} [\theta(t) - 1 - \ln \theta(t)], \quad \theta(t) \equiv \frac{T(t)}{T_b}. \end{aligned} \quad (12b)$$

Both \mathcal{D}^{kin} and \mathcal{D}^{LE} are positive definite [77]. To split \mathcal{D} into the sum of \mathcal{D}^{kin} and \mathcal{D}^{LE} , we have employed that the average of the kinetic energy with $f(\mathbf{v}, t)$ is the same

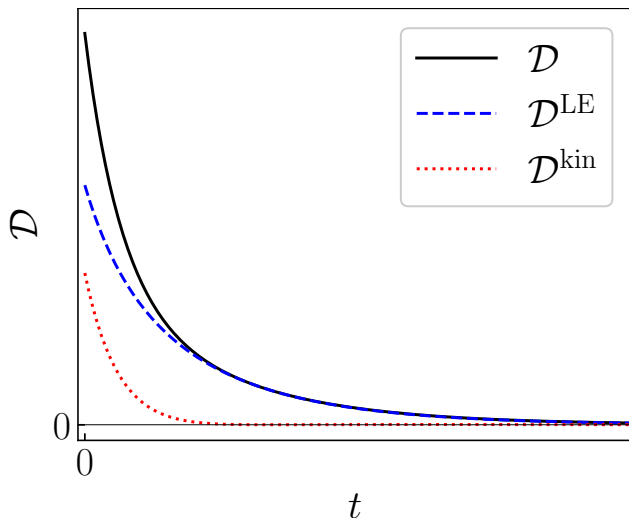


FIG. 2. Sketch showing a typical evolution of the total KLD (solid line), its LE contribution (dashed line), and its kinetic contribution (dotted line).

as with $f^{\text{LE}}(\mathbf{v}; T(t))$. A generalization of this idea makes it possible to define a nonequilibrium temperature and an analogous splitting of \mathcal{D} in quite a general class of systems, see Sec. VII for further details.

The first contribution to the total \mathcal{D} , \mathcal{D}^{kin} , is a measure of the departure of the true VDF from the LE one, and depends explicitly on time through the whole VDF $f(\mathbf{v}, t)$. In contrast, the second contribution \mathcal{D}^{LE} measures the deviation of the LE state from the asymptotic equilibrium state and only depends on time through the nonequilibrium temperature $T(t)$, namely on the temperature ratio $\theta(t)$. More specifically, \mathcal{D}^{LE} monotonically increases as $|\theta - 1|$ increases in the domains $\theta > 1$ and $\theta < 1$ separately. Figure 2 presents a sketch of the temporal evolution of \mathcal{D} and its two contributions, \mathcal{D}^{LE} and \mathcal{D}^{kin} [78].

The TME and EME can be directly related if the crossing comes about in the hydrodynamic regime, since therein $\mathcal{D}^{\text{kin}} \approx 0$ and $\mathcal{D}(t) \approx \mathcal{D}^{\text{LE}}(\theta(t))$ —which is a function of temperature only, as explicitly stated by our notation. Therefore, the TME and EME become equivalent during the hydrodynamic stage, and $t_\theta \simeq t_{\mathcal{D}}$. However, we will show that in most situations the ME occurs during the kinetic stage, the contribution \mathcal{D}^{kin} is then relevant, and the physical picture is much more complex. In fact, the two-stage relaxation picture may even break down under certain conditions, as discussed in Ref. [79].

III. EVOLUTION EQUATIONS

Multiplying both sides of Eq. (3) by v^2 and integrating over velocity one readily obtains the evolution equation

for the time-dependent temperature,

$$\frac{\dot{T}}{\zeta_0} = -2(T - T_b) \left[1 + (d+2)\gamma \frac{T}{T_b} \right] - 2(d+2)\gamma \frac{T^2}{T_b} a_2, \quad (13)$$

where

$$a_2(t) \equiv \frac{d}{d+2} \frac{\langle v^4 \rangle}{\langle v^2 \rangle^2} - 1 \quad (14)$$

is the excess kurtosis.

Using as unit of time the mean free time—average time between collisions—at equilibrium,

$$\tau_b = \frac{K_d}{g_c n \sigma^{d-1} \sqrt{2k_B T_b/m}}, \quad K_d \equiv \frac{\sqrt{2}\Gamma(d/2)}{\pi^{\frac{d-1}{2}}}, \quad (15)$$

the dimensionless time t^* and zero-velocity drag coefficient ζ_0^* can be defined as

$$t^* = t/\tau_b, \quad \zeta_0^* = \zeta_0 \tau_b. \quad (16)$$

The parameter ζ_0^* measures the relative relevance of the drag force (i.e., the interactions between the particles and the background fluid) and hard-sphere binary collisions. The limit $\zeta_0^* \rightarrow 0$ corresponds to negligible drag force, where the EFPE reduces to the Enskog equation. The limit $\zeta_0^* \rightarrow \infty$ corresponds to negligible collisions, where the EFPE reduces to the Fokker–Planck equation [80]. In this work, we typically consider the value $\zeta_0^* = 1$, for which the drag force and binary collisions are comparable and act over the same timescale. Note that both the drag force and binary collisions drive by themselves the system to equilibrium, independently of the magnitude of the other interaction, with the entropic distance monotonically decreasing to zero [81].

In the remainder of the paper we employ dimensionless quantities. Dimensionless temperature is identified with the temperature ratio θ defined in Eq. (12b). For simplicity, henceforth the stars on t^* and ζ_0^* are dropped. The evolution equation for the temperature, Eq. (13), thus reads

$$\frac{\dot{\theta}}{\zeta_0} = -2(\theta - 1) [1 + (d+2)\gamma\theta] - 2(d+2)\gamma\theta^2 a_2. \quad (17)$$

Notice that one gets Newton’s cooling law $\dot{\theta} = -2\zeta_0(\theta - 1)$ in the linear case $\gamma = 0$. However, if $\gamma \neq 0$, then the evolution of temperature is coupled to that of the fourth-degree moment $\langle v^4 \rangle$ through a_2 . Next, the evolution equation for $\langle v^4 \rangle$ stemming from the EFPE, Eq. (3), is coupled to the sixth-degree moment $\langle v^6 \rangle$ due to the nonlinear drag term and to all the moments $\langle v^\ell \rangle$ due to the collision term, and so on. Thus, the full evolution of $\theta(t)$ is coupled to the infinite hierarchy of moment equations, which are derived in Appendix B by introducing a Sonine expansion of the VDF. By retaining only the first two terms in the expansion, which involve the excess kurtosis (or fourth-order cumulant) a_2 and the sixth-order

cumulant a_3 ,

$$a_3(t) = 1 + 3a_2 - \frac{d^2}{(d+2)(d+4)} \frac{\langle v^6 \rangle}{\langle v^2 \rangle^3}, \quad (18)$$

and neglecting nonlinear terms in the cumulants one gets

$$\begin{aligned} \frac{\dot{a}_2}{\zeta_0} = & -8\gamma(\theta - 1) + 4 \left[2\gamma - (d+8)\gamma\theta - \frac{1}{\theta} \right] a_2 \\ & + 4(d+4)\gamma\theta a_3 - \frac{8(d-1)\sqrt{\theta}}{d(d+2)\zeta_0} \left(a_2 - \frac{a_3}{4} \right), \end{aligned} \quad (19a)$$

$$\begin{aligned} \frac{\dot{a}_3}{\zeta_0} = & -24\gamma(2-3\theta)a_2 + 6 \left[4\gamma - (d+14)\gamma\theta - \frac{1}{\theta} \right] a_3 \\ & + \frac{\sqrt{\theta}}{\zeta_0} \frac{3(d-1)}{d(d+2)(d+4)} [4a_2 - (4d+19)a_3]. \end{aligned} \quad (19b)$$

Equations (17) and (19) make a closed set of three coupled differential equations, nonlinear in the temperature but linear in the cumulants.

In this paper, we consider two Sonine approximations. The roughest approximation consists of neglecting a_3 , setting $a_3 = 0$ in Eq. (19a), and dealing then with Eqs. (17) and (19a) for the pair (θ, a_2) . Here, we term this approach the basic Sonine approximation (BSA) [82]. A more sophisticated theory is obtained by keeping a_3 and dealing then with Eqs. (17) and (19). We term this approach the extended Sonine approximation (ESA) [83].

IV. THERMAL VERSUS ENTROPIC MPEMBA EFFECTS

A. Heuristic arguments

Now we proceed to study the ME in the theoretical framework of the Sonine approximations we have just introduced. To start with, let us consider two samples (A and B) at the *same* initial temperatures $\theta_A(0) \equiv \theta_A^0$ and $\theta_B(0) \equiv \theta_B^0$, above the equilibrium value, i.e., $\theta_A^0 = \theta_B^0 > 1$. According to Eq. (17), the initial slopes $\dot{\theta}_A(0)$ and $\dot{\theta}_B(0)$ satisfy the inequality $\dot{\theta}_A(0) < \dot{\theta}_B(0)$ if $a_{2A}(0) \equiv a_{2A}^0 > a_{2B}(0) \equiv a_{2B}^0$, in which case sample A is expected to reach equilibrium before sample B. It must be brought to bear that the latter statement is true if $\theta(t) - 1$ keeps its initial sign along the whole relaxation to equilibrium, a condition that is assumed throughout this section. Exceptions to this fact, due to the overshoot of θ with respect to its equilibrium value, are discussed in Sec. V.

In order to analyze the TME described in Sec. I, let us take now $\theta_A^0 > \theta_B^0 > 1$. As discussed above, $\theta_A(0) < \dot{\theta}_B(0)$ if $a_{2A}^0 > a_{2B}^0$. In that way, it can be expected that, by a convenient choice of the initial-condition values (θ_A^0, a_{2A}^0) and (θ_B^0, a_{2B}^0) , the evolution curves $\theta_A(t)$ and $\theta_B(t)$ intersect at a certain crossover time t_θ . That

is, $\theta_A(t_\theta) = \theta_B(t_\theta)$ and $\dot{\theta}_A(t_\theta) < \dot{\theta}_B(t_\theta)$, which entails $a_{2A}(t_\theta) > a_{2B}(t_\theta)$ and $1 < \theta_A(t) < \theta_B(t)$ for $t > t_\theta$. This is the typical framework for the emergence of the (direct) TME in the kinetic description [36, 37, 39].

The inverse TME is analogous, except that, instead of $\theta_A^0 > \theta_B^0 > 1$, one now has $\theta_A^0 < \theta_B^0 < 1$. If now $a_{2B}^0 > a_{2A}^0$, then $\dot{\theta}_B(0) < \dot{\theta}_A(0)$, so that it is in principle possible that the evolution curve $\theta_A(t)$ intersects $\theta_B(t)$ at a certain crossover time t_θ .

Note that, without loss of generality, we denote by A the sample with an initial temperature farther from the equilibrium one, both in the direct and inverse TME. Thus, the necessary (but, of course, not sufficient) conditions for the direct and inverse TME are $a_{2A}^0 > a_{2B}^0$ and $a_{2B}^0 > a_{2A}^0$, respectively.

In this work, we analyze both the TME and the EME. In the latter, it is the evolution curves of the relative entropy \mathcal{D} that intersect at a certain time $t_{\mathcal{D}}$, as described in Sec. I [84]. In particular, we want to understand whether the TME implies the EME or not. Also, when both the TME and the EME are present, we would like to investigate the relation between the crossing times t_θ and $t_{\mathcal{D}}$.

Let us address the questions above by simple heuristic arguments. First, we consider the case in which the further from equilibrium sample in the kinetic approach (A) is also the further from equilibrium in the entropic approach, i.e., $\mathcal{D}_A^0 > \mathcal{D}_B^0$. Therein, the existence of the TME implies that of the EME, and vice versa, as shown below. Note that $\mathcal{D}_A^0 > \mathcal{D}_B^0$ if \mathcal{D}^0 increases with $|\theta^0 - 1|$. This is indeed true for the LE contribution \mathcal{D}^{LE} , but not necessarily so for the total KLD \mathcal{D} if the kinetic contribution \mathcal{D}^{kin} plays a relevant role.

For the direct TME, we have $\theta_A^0 > \theta_B^0 > 1$ and $\mathcal{D}_A^0 > \mathcal{D}_B^0$. If the TME exists, then one has $\theta_B(t) > \theta_A(t) > 1$ after the crossover. In particular, this holds for sufficiently long times belonging to the hydrodynamic stage, where both $\mathcal{D}_A^{\text{kin}}$ and $\mathcal{D}_B^{\text{kin}}$ are negligible, and thus one has $\mathcal{D}_B(t) > \mathcal{D}_A(t)$ (EME) in the same stage. Reciprocally, if the EME exists, then $\mathcal{D}_B(t) > \mathcal{D}_A(t)$ in the hydrodynamic stage after the crossover, implying $\theta_B(t) > \theta_A(t) > 1$ (TME) in the same regime. An analogous reasoning applies to the inverse TME, i.e., $1 > \theta_B^0 > \theta_A^0$ and $\mathcal{D}_A^0 > \mathcal{D}_B^0$.

Provided that the TME and EME are present, the argument above does not tell us the relative positioning of the crossover times t_θ and $t_{\mathcal{D}}$, i.e., whether $t_\theta > t_{\mathcal{D}}$ or $t_\theta < t_{\mathcal{D}}$. Let us start by considering that the direct TME takes place at t_θ . Therefore, we have that $\mathcal{D}_A^{\text{LE}}(t_\theta) = \mathcal{D}_B^{\text{LE}}(t_\theta)$ and only the kinetic part contributes to the KLD difference at t_θ , $\mathcal{D}_A(t_\theta) - \mathcal{D}_B(t_\theta) = \mathcal{D}_A^{\text{kin}}(t_\theta) - \mathcal{D}_B^{\text{kin}}(t_\theta)$. This implies that $\mathcal{D}_A(t_\theta) < \mathcal{D}_B(t_\theta)$ (and hence $t_{\mathcal{D}} < t_\theta$) if $\mathcal{D}_A^{\text{kin}}(t_\theta) < \mathcal{D}_B^{\text{kin}}(t_\theta)$, while $\mathcal{D}_A(t_\theta) > \mathcal{D}_B(t_\theta)$ (and hence $t_{\mathcal{D}} > t_\theta$) otherwise.

For the sake of simplicity, and to go beyond the generic analysis of the previous paragraph, let us assume that the values of the excess kurtoses at the crossover time t_θ are small enough as to approximate $\mathcal{D}^{\text{kin}} \propto a_2^2$. The

TABLE I. Summary of possible cases regarding the occurrence of the TME and the EME.

Case	Type of ME	Initial condition	If ...	then ...
ET1	Direct TME & EME	$\theta_A^0 > \theta_B^0 > 1$, $a_{2A}^0 > a_{2B}^0$, $\mathcal{D}_A^0 > \mathcal{D}_B^0$	$ a_{2A}(t_\theta) < a_{2B}(t_\theta) $	$t_{\mathcal{D}} < t_\theta$
TE1	Direct TME & EME	$\theta_A^0 > \theta_B^0 > 1$, $a_{2A}^0 > a_{2B}^0$, $\mathcal{D}_A^0 > \mathcal{D}_B^0$	$ a_{2A}(t_\theta) > a_{2B}(t_\theta) $	$t_{\mathcal{D}} > t_\theta$
ET2	Inverse TME & EME	$\theta_A^0 < \theta_B^0 < 1$, $a_{2A}^0 < a_{2B}^0$, $\mathcal{D}_A^0 > \mathcal{D}_B^0$	$ a_{2A}(t_\theta) < a_{2B}(t_\theta) $	$t_{\mathcal{D}} < t_\theta$
TE2	Inverse TME & EME	$\theta_A^0 < \theta_B^0 < 1$, $a_{2A}^0 < a_{2B}^0$, $\mathcal{D}_A^0 > \mathcal{D}_B^0$	$ a_{2A}(t_\theta) > a_{2B}(t_\theta) $	$t_{\mathcal{D}} > t_\theta$
T1	Direct TME	$\theta_A^0 > \theta_B^0 > 1$, $a_{2A}^0 > a_{2B}^0$	$\mathcal{D}_B^0 > \mathcal{D}_A^0$	No EME
T2	Inverse TME	$\theta_A^0 < \theta_B^0 < 1$, $a_{2A}^0 < a_{2B}^0$	$\mathcal{D}_B^0 > \mathcal{D}_A^0$	No EME
E1	EME	$\mathcal{D}_B^0 > \mathcal{D}_A^0$	$\theta_A^0 > \theta_B^0 > 1$	No Direct TME
E2	EME	$\mathcal{D}_B^0 > \mathcal{D}_A^0$	$\theta_A^0 < \theta_B^0 < 1$	No Inverse TME

proportionality constant may depend on the details of the VDF—see Eq. (24) below for the specific example of a gamma distribution. Within this approximation, the first case, $t_{\mathcal{D}} < t_\theta$, is expected if $|a_{2A}(t_\theta)| < |a_{2B}(t_\theta)|$, while the second case, $t_{\mathcal{D}} > t_\theta$, is expected if $|a_{2A}(t_\theta)| > |a_{2B}(t_\theta)|$. Both scenarios are possible, even recalling that $a_{2A}(t_\theta) > a_{2B}(t_\theta)$ is a necessary condition to have the TME, because the sign of the excess kurtoses of samples A and B may be different. For the case of the inverse TME, the sign of $t_{\mathcal{D}} - t_\theta$ coincides again with that of $|a_{2A}(t_\theta)| - |a_{2B}(t_\theta)|$.

The different possibilities analyzed above for the case $\mathcal{D}_A^0 > \mathcal{D}_B^0$ are summarized in Table I, specifically as cases labeled ET1, TE1 (for the direct ME) and ET2, TE2 (for the inverse ME).

Now we move onto the situation in which the further from equilibrium sample in the kinetic approach (A) is, however, the closer to equilibrium in the entropic approach, $\mathcal{D}_A^0 < \mathcal{D}_B^0$. On account of Eq. (12b), the condition $\mathcal{D}_B^0 > \mathcal{D}_A^0$ requires

$$\mathcal{D}_B^{\text{kin},0} - \mathcal{D}_A^{\text{kin},0} > \frac{d}{2} \left(\theta_A^0 - \theta_B^0 - \ln \frac{\theta_A^0}{\theta_B^0} \right) > 0. \quad (20)$$

Additional cases are possible, which are labeled as T1, T2, E1, and E2 in Table I. The TME and the EME are no longer biunivocally related. For example, in the T1 case, the direct TME is present but no genuine EME takes place: $\theta_A^0 > \theta_B^0 > 1$ and $\theta_B(t) > \theta_A(t) > 1$ for $t > t_\theta$, but $\mathcal{D}_B > \mathcal{D}_A$ both initially and for asymptotically long times. Note, however, that this does not prevent the difference $\mathcal{D}_B(t) - \mathcal{D}_A(t)$ from changing its sign an even number of times during the transient relaxation.

To fix ideas and for further use, let us take the VDF corresponding to a gamma distribution [85] for the probability density of the variable $x = c^2$. Using the condition $\langle c^2 \rangle = \frac{d}{2}$, the reduced VDF associated with the gamma distribution reads

$$\phi(\mathbf{c}) = \pi^{-d/2} \frac{\Gamma(\frac{d}{2}) z^{d/2}}{\Gamma(\frac{dz}{2})} c^{d(z-1)} e^{-zc^2}, \quad z \equiv \frac{1}{1 + \frac{d+2}{2} a_2}. \quad (21)$$

Note that this includes the LE distribution, Eq. (B10), as the special case $a_2 = 0$. Thus, the deviations of the distribution (21) from LE are monitored by the excess

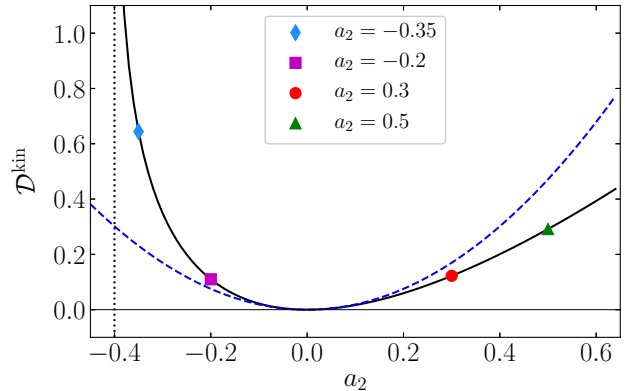


FIG. 3. Dependence of \mathcal{D}^{kin} with a_2 for a gamma distribution. Specifically, we plot the exact expression (solid line), given by Eq. (23), and the small $|a_2|$ approximation (dotted line), given by Eq. (24), for $d = 3$. Symbols correspond to the particular values at $a_2 = -0.35, -0.20, 0.30$, and 0.50 considered in Table II.

kurtosis a_2 only. In particular, the sixth cumulant is given by

$$a_3 = \frac{4}{d+4} a_2 \left(1 - \frac{d+2}{2} a_2 \right). \quad (22)$$

The KLD of the gamma distribution with respect to the LE one is [86]

$$\mathcal{D}^{\text{kin}} = \frac{d}{2} \left\{ \ln z + (z-1) \left[\psi \left(\frac{dz}{2} \right) - 1 \right] \right\} + \ln \frac{\Gamma(\frac{d}{2})}{\Gamma(\frac{dz}{2})}, \quad (23)$$

in which $\psi(x) = d \ln \Gamma(x) / dx$ is the digamma function [87]. For small $|a_2|$, one has

$$\mathcal{D}^{\text{kin}} \approx \frac{d(d+2)^2}{16} \left[\frac{d}{2} \psi' \left(\frac{d}{2} \right) - 1 \right] a_2^2, \quad (24)$$

where $\psi'(x) \equiv d\psi(x)/dx$.

The dependence of \mathcal{D}^{kin} , as given by Eq. (23), as a function of a_2 in the three-dimensional case ($d = 3$) is shown in Fig. 3. We observe that \mathcal{D}^{kin} grows more rapidly for negative than for positive values of a_2 , exhibiting a vertical asymptote at $a_2 = -2/(d+2)$, which corresponds to $z \rightarrow \infty$.

B. Linearized analysis

To provide a simple, but yet more quantitative, study, in the remainder of this section (and also in Sec. V) we adopt the linearization scheme put forward in Ref. [36]. The starting point is the BSA described by Eqs. (17) and (19a), setting $a_3 \rightarrow 0$ in the latter. Furthermore, the temperature ratio θ is linearized around a reference value θ_r close to $\theta^0 \equiv \theta(0)$. The solution of the resulting set of two differential equations is [36]

$$\begin{aligned} \theta(t) = & B_1 + [A_{11}(\theta^0 - B_1) - A_{12}(a_2^0 - B_2)] e^{-\lambda_- t} \\ & - [(A_{11} - 1)(\theta^0 - B_1) - A_{12}(a_2^0 - B_2)] e^{-\lambda_+ t}, \end{aligned} \quad (25a)$$

$$\begin{aligned} a_2(t) = & B_2 + [A_{22}(a_2^0 - B_2) - A_{21}(\theta^0 - B_1)] e^{-\lambda_- t} \\ & - [(A_{22} - 1)(a_2^0 - B_2) - A_{21}(\theta^0 - B_1)] e^{-\lambda_+ t}, \end{aligned} \quad (25b)$$

in which $a_2^0 \equiv a_2(0)$, and the expressions of the parameters λ_{\pm} , B_i , and A_{ij} can be found in Appendix C. We refer to Eqs. (25) as the linearized basic Sonine approximation (LBSA). When using the LBSA to investigate the ME, we are assuming that $\theta(t)$ is close to θ_r , which in turn is close to θ^0 . This entails that the LBSA is expected to be applicable to the kinetic stage only—i.e., when the ME comes about for short times.

The LBSA can be applied to the evolution of the two samples A and B with the convenient choice $\theta_r = \theta_B^0$ [36]. It is then straightforward to find the crossover time t_θ as

$$t_\theta = \frac{1}{\lambda_+ - \lambda_-} \ln \left(1 + \frac{A_{11}^{-1}}{R_{\max}^0/R^0 - 1} \right), \quad (26)$$

where

$$R^0 \equiv \frac{\theta_A^0 - \theta_B^0}{a_{2A}^0 - a_{2B}^0}, \quad R_{\max}^0 \equiv \frac{A_{12}}{A_{11}}. \quad (27)$$

Therefore, in the LBSA, the crossover time t_θ depends on the set of four initial values θ_A^0 , a_{2A}^0 , θ_B^0 , and a_{2B}^0 only through the ratio R^0 . Moreover, Eq. (26) is meaningful only if

$$0 < R^0 < R_{\max}^0. \quad (28)$$

Otherwise, no TME—either direct or inverse—exists.

The determination of the crossover time $t_{\mathcal{D}}$ is much more involved, even in the simple LBSA. It is obtained as the solution of a transcendental equation and the solution depends on θ_A^0 , a_{2A}^0 , θ_B^0 , and a_{2B}^0 . The locus separating the region where $t_{\mathcal{D}} < t_\theta$ from the region where $t_{\mathcal{D}} > t_\theta$ is approximately given by the condition $|a_{2A}(t_\theta)| = |a_{2B}(t_\theta)|$; the sign of $t_{\mathcal{D}} - t_\theta$ is the same as that of $|a_{2A}(t_\theta)| - |a_{2B}(t_\theta)|$ —as discussed in the previous section. See cases ET1, TE1, ET2, and TE2 in Table I. Furthermore, cases T1, T2, E1, and E2 are possible if the initial values of the KLD cross the locus $\mathcal{D}_A^0 = \mathcal{D}_B^0$, as

TABLE II. Four representative choices for the initial values a_{2A}^0 and a_{2B}^0 ($d = 3$). The numerical values of \mathcal{D}^{kin} , as given by Eq. (23) with $d = 3$, are also included. The sixth column gives the cases (see Table I) that, in principle, are associated with each pair (a_{2A}^0, a_{2B}^0) . However, some of them (enclosed in parentheses) are not actually observed (see Fig. 4).

Label	a_{2A}^0	a_{2B}^0	$\mathcal{D}_A^{\text{kin},0}$	$\mathcal{D}_B^{\text{kin},0}$	Cases
I	0.50	-0.35	0.292	0.644	ET1, (TE1), T1, E1, E2
II	0.50	-0.20	0.292	0.110	ET1, TE1
III	-0.35	0.30	0.644	0.122	ET2, TE2
IV	-0.20	0.50	0.110	0.292	(ET2), (TE2), T2, E1, E2

summarized in Table I and described in Sec. IV A. If the locus $\mathcal{D}_A^0 = \mathcal{D}_B^0$ happens to separate regions ET1 and T1 (or ET2 and T2), then one has $t_{\mathcal{D}} \rightarrow 0$ on the locus, so that $0 < t_{\mathcal{D}} < t_\theta$ in region ET1 (or ET2) and formally $t_{\mathcal{D}} < 0 < t_\theta$ in region T1 (or T2).

C. Illustrative examples

Let us choose the four representative pairs (a_{2A}^0, a_{2B}^0) presented in Table II. Since the scenarios ET1 and TE1 described in Table I require $a_{2A}^0 > a_{2B}^0$, they are *in principle* feasible for the pairs I and II. Analogously, the scenarios ET2 and TE2 might be possible for the pairs III and IV. Next, by assuming the initial VDF has the gamma form, Eq. (21), we have $\mathcal{D}_B^{\text{kin},0} > \mathcal{D}_A^{\text{kin},0}$ for the pairs I and IV, but not for the pairs II and III; in view of Eq. (20), we conclude that, *in principle*, cases T1, E1, and E2 are possible for pair I and cases T2, E1, and E2 for pair IV.

The phase diagrams predicted by the LBSA are shown in Fig. 4 for $\zeta_0 = 1$, $\gamma = 0.1$, and $d = 3$. We observe that, at least for that choice of the parameters, case TE1 is absent for the class of initial conditions I, while cases ET2 and TE2 are absent for the class of initial conditions IV. This confirms that the initial conditions shown in the third column of Table I for the cases ET1, TE1, ET2, and TE2 represent necessary—but not sufficient—conditions for their occurrence, the actual realization of those scenarios depending on the evolution of $a_{2A}(t)$ and $a_{2B}(t)$.

The time evolution of the differences

$$\Delta\mathcal{D} \equiv \mathcal{D}_A - \mathcal{D}_B, \quad \Delta\mathcal{D}^{\text{LE}} \equiv \mathcal{D}_A^{\text{LE}} - \mathcal{D}_B^{\text{LE}} \quad (29)$$

for the representative points indicated in Fig. 4 are displayed in Figs. 5–8, where the difference $\Delta\mathcal{D}^{\text{kin}} = \mathcal{D}_A^{\text{kin}} - \mathcal{D}_B^{\text{kin}} = \Delta\mathcal{D} - \Delta\mathcal{D}^{\text{LE}}$ is also included. The change of sign of $\mathcal{D}_A^{\text{LE}} - \mathcal{D}_B^{\text{LE}}$ and $\mathcal{D}_A - \mathcal{D}_B$ during their evolution signals the presence of the TME and EME, respectively. Here, we made an extra ansatz to evaluate $\mathcal{D}^{\text{kin}}(t)$. As we are working with an initial gamma distribution and the final equilibrium state is a particular case of such a distribution—with $a_2 = 0$, we have assumed that the VDF during its time evolution is sufficiently close to a

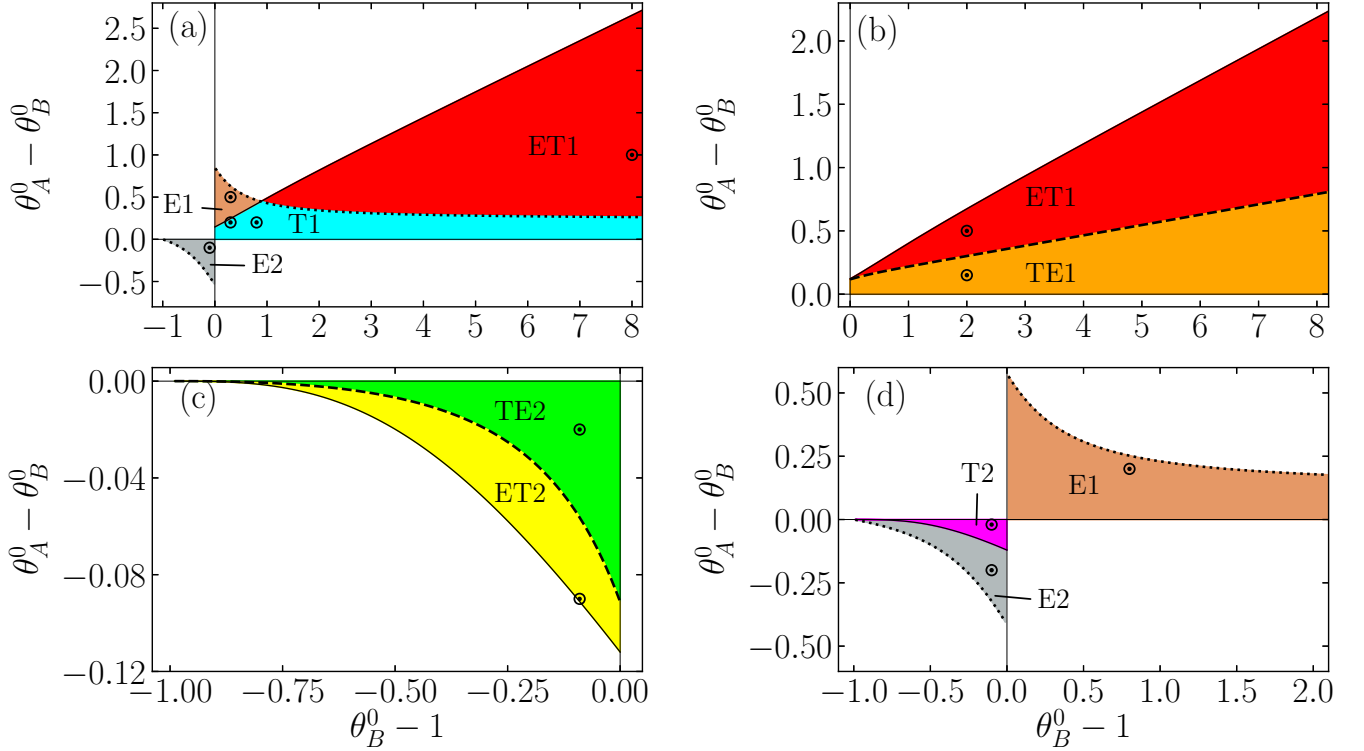


FIG. 4. Phase diagrams in the representation $\theta_A^0 - \theta_B^0$ vs $\theta_B^0 - 1$. Specifically, they are plotted for $\zeta_0 = 1$, $\gamma = 0.1$, $d = 3$, and the four representative choices of (a_{2A}^0, a_{2B}^0) displayed in Table II: (a) I, (b) II, (c) III, and (d) IV. The solid, dashed, and dotted lines represent the loci $R^0 = R_{\max}^0$, $t_\theta = t_D$, and $\mathcal{D}_A^0 = \mathcal{D}_B^0$, respectively. The labels in each region correspond to the cases described in Table I and the circles represent the specific examples considered in Figs. 5–8. Note that $\theta_A^0 > \theta_B^0 > 1$ and $\theta_A^0 < \theta_B^0 < 1$ refer to the direct TME and inverse TME, respectively.

gamma distribution so as to estimate $\mathcal{D}^{\text{kin}}(t)$ by Eq. (23) with an excess kurtosis $a_2(t)$ given by Eq. (25b).

Figures 5(b) and 5(c) are both examples of the scenario T1 for the class of initial conditions I. In Fig. 5(b), where $(\theta_B^0 - 1, \theta_A^0 - \theta_B^0) = (0.8, 0.2)$ [see Fig. 4(a)], the difference $\mathcal{D}_A^0 - \mathcal{D}_B^0$ presents a negative local maximum. When moving horizontally in Fig. 4(a) to the point $(\theta_B^0 - 1, \theta_A^0 - \theta_B^0) = (0.3, 0.2)$, however, Fig. 5(c) shows that the local maximum of $\mathcal{D}_A^0 - \mathcal{D}_B^0$ becomes positive and $\mathcal{D}_A^0 - \mathcal{D}_B^0$ vanishes twice during the time evolution. While interesting, this does not qualify as an EME because, as already said above Eq. (20), $\mathcal{D}_B > \mathcal{D}_A$ both initially and for asymptotically long times. Next, moving vertically in Fig. 4(a) to the point $(\theta_B^0 - 1, \theta_A^0 - \theta_B^0) = (0.3, 0.5)$, the local maximum observed in Fig. 5(d) is again positive but there is a single crossing $\mathcal{D}_A^0 - \mathcal{D}_B^0 = 0$, which results in the E1 scenario.

V. OVERSHOOT MPEMBA EFFECT

In Sec. IV, we have assumed that, even though the evolution of $\theta(t)$ may not be monotonic, $\theta(t) - 1$ does not change sign, i.e., the temperature does not overshoot the equilibrium value. However, such an overshoot $\theta(t_O) = 1$

at a finite time t_O is possible. In general, $a_2(t_O) \neq 0$, and Eq. (17) shows that $\dot{\theta}(t_O)/\zeta_0\gamma = -2(d+2)a_2(t_O) \neq 0$. As a consequence, starting from $\theta^0 > 1$, $\theta(t) - 1$ develops a hump with a negative minimum if $a_2(t_O) > 0$; analogously, starting from $\theta^0 < 1$ and if $a_2(t_O) < 0$, $\theta(t) - 1$ develops a hump with a positive maximum, reminiscent of the Kovacs effect [37, 88–94]. We will refer to this crossover $\theta(t_O) = 1$ and subsequent hump, either positive or negative, as an overshoot phenomenon.

Given the fact that the relaxation of $a_2(t)$ is generally much faster than that of $\theta(t)$, at least if $\theta^0 = O(1)$ [37], it is reasonable to expect that the overshoot effect requires initial values $|\theta^0 - 1| \ll 1$, unless $|a_2^0|$ is unphysically large. This suggests a theoretical treatment based on the LBSA (25) with $\theta_r \rightarrow 1$, i.e.,

$$\theta(t) = 1 + [\bar{A}_{11}(\theta^0 - 1) - \bar{A}_{12}a_2^0] e^{-\bar{\lambda}_- t} - [(\bar{A}_{11} - 1)(\theta^0 - 1) - \bar{A}_{12}a_2^0] e^{-\bar{\lambda}_+ t}, \quad (30a)$$

$$a_2(t) = [\bar{A}_{22}a_2^0 - \bar{A}_{21}(\theta^0 - 1)] e^{-\bar{\lambda}_- t} - [(\bar{A}_{22} - 1)a_2^0 - \bar{A}_{21}(\theta^0 - 1)] e^{-\bar{\lambda}_+ t}, \quad (30b)$$

where overlined quantities refer to their values at $\theta_r = 1$. Following the same methodology as in Eqs. (26) and (27),

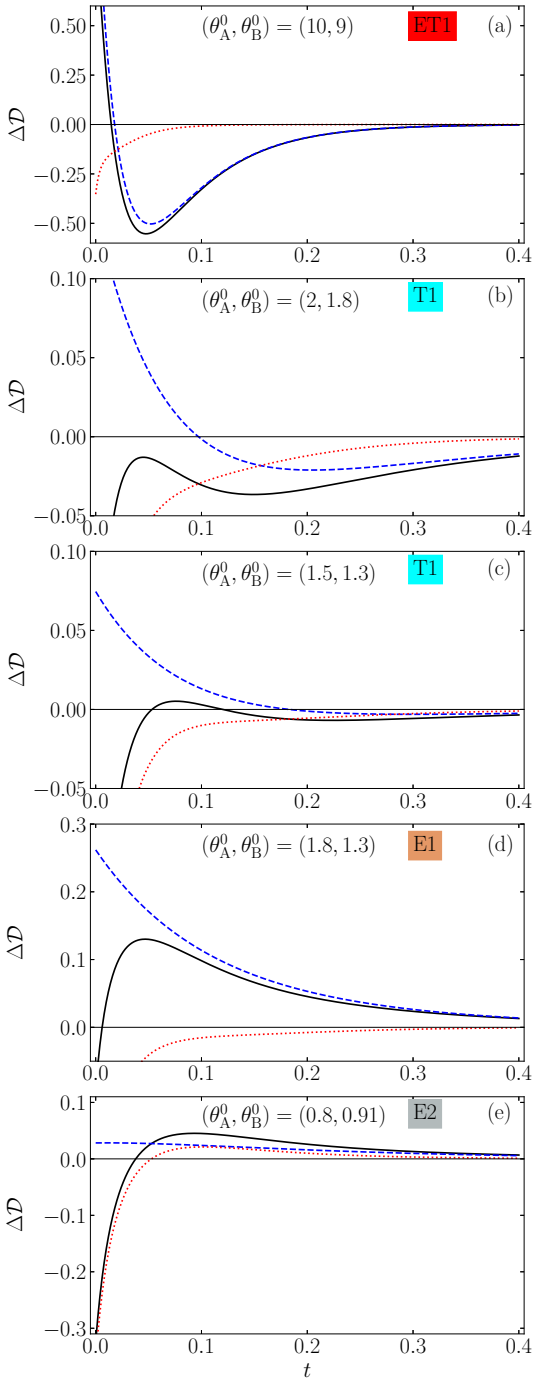


FIG. 5. Time evolution of the difference of the relative entropies for the representative initial condition I in Table II, $(a_{2A}^0, a_{2B}^0) = (0.50, -0.35)$. Parameter values are $\zeta_0 = 1$, $\gamma = 0.1$, $d = 3$. Specifically, we represent $\mathcal{D}_A^{\text{kin}} - \mathcal{D}_B^{\text{kin}}$ (dotted lines), $\mathcal{D}_A^{\text{LE}} - \mathcal{D}_B^{\text{LE}}$ (dashed lines), and $\mathcal{D}_A - \mathcal{D}_B$ (solid lines) for different pairs of initial temperatures, namely: (a) $(\theta_B^0 - 1, \theta_A^0 - \theta_B^0) = (8, 1)$, (b) $(\theta_B^0 - 1, \theta_A^0 - \theta_B^0) = (0.8, 0.2)$, (c) $(\theta_B^0 - 1, \theta_A^0 - \theta_B^0) = (0.3, 0.2)$, (d) $(\theta_B^0 - 1, \theta_A^0 - \theta_B^0) = (0.3, 0.5)$, and (e) $(\theta_B^0 - 1, \theta_A^0 - \theta_B^0) = (-0.09, -0.11)$. Panels (a), (b), (c), (d) and (e) represent examples of cases ET1, T1, T1, E1, and E2, respectively [see Fig. 4(a)].

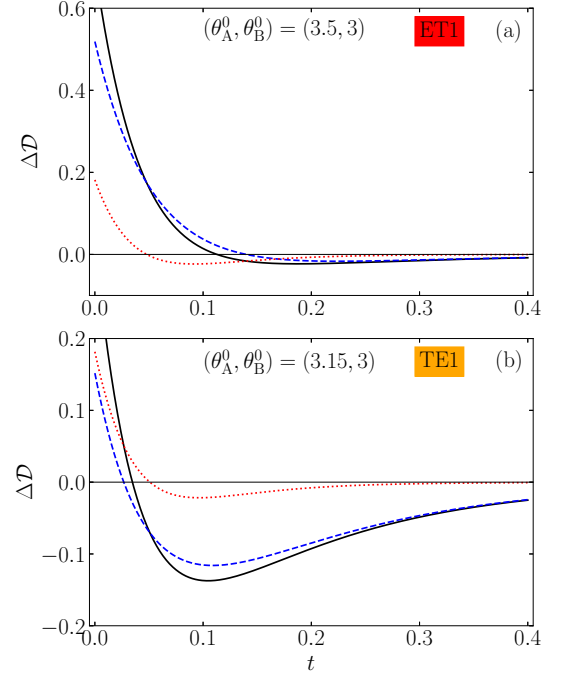


FIG. 6. Same as in Fig. 5, but now for the representative initial condition II in Table II, $(a_{2A}^0, a_{2B}^0) = (0.50, -0.20)$. Here, initial conditions for the temperatures are: (a) $(\theta_B^0 - 1, \theta_A^0 - \theta_B^0) = (2.0, 0.5)$ and (b) $(\theta_B^0 - 1, \theta_A^0 - \theta_B^0) = (2.00, 0.15)$. Panels (a) and (b) represent examples of cases ET1 and TE1, respectively [see Fig. 4(b)].

we find

$$t_O = \frac{1}{\lambda_+ - \lambda_-} \ln \left[1 + \frac{\bar{A}_{11}^{-1}}{\bar{R}_{\max}^0 a_2^0 / (\theta^0 - 1) - 1} \right], \quad (31)$$

where

$$\bar{R}_{\max}^0 \equiv \frac{\bar{A}_{12}}{\bar{A}_{11}}. \quad (32)$$

Therefore, according to the LBSA, the overshoot effect appears if

$$0 < \frac{\theta^0 - 1}{a_2^0} < \bar{R}_{\max}^0. \quad (33)$$

It is interesting to look into the possible change of the ME phenomenology brought about by the overshoot-induced humps. As we show below, the existence of humps may make it necessary to change the preconception of considering the TME present only when the evolution curves of the temperature of the two samples intersect. To be more specific, we consider, as before, samples A and B with A being the initially hotter, i.e., $\theta_A^0 > \theta_B^0 > 1$. Let us assume that the colder sample B fulfills condition (33) but the hotter sample does not. In that case, $\theta_B(t)$ might not be crossed by the curve $\theta_A(t)$, which remains always above the equilibrium temperature, and yet relax more slowly to equilibrium than A

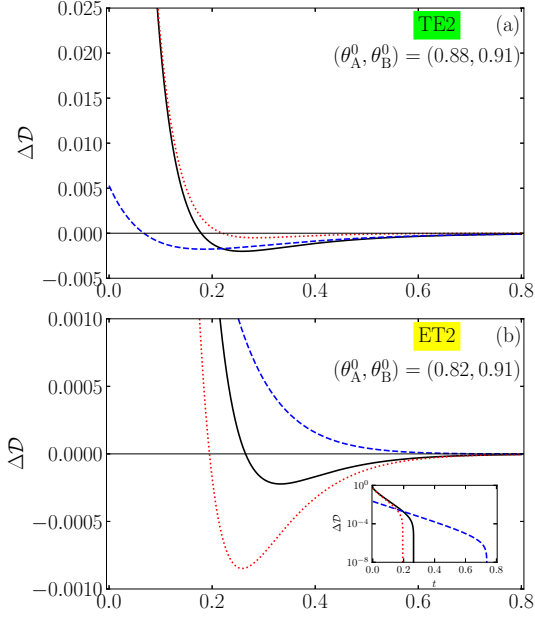


FIG. 7. Same as in Fig. 5, but now for the representative initial condition III in Table II, $(a_{2A}^0, a_{2B}^0) = (-0.35, 0.30)$. In this case, the initial conditions for the temperatures chosen are: (a) $(\theta_B^0 - 1, \theta_A^0 - \theta_B^0) = (-0.09, -0.03)$ and (b) $(\theta_B^0 - 1, \theta_A^0 - \theta_B^0) = (-0.09, -0.09)$. Panels (a) and (b) represent examples of cases TE2 and ET2, respectively [see Fig. 4(c)]. Note that $\Delta\mathcal{D}$ is plotted in logarithmic scale in the inset of panel (b) to favor the perception of the crossover times, at which $\Delta\mathcal{D}$ vanishes.

but from below. We could then say that a (direct) TME is present without the existence of a standard crossover time t_θ , provided that a crossover between the LE KLD curves $\mathcal{D}_A^{\text{LE}}(t)$ and $\mathcal{D}_B^{\text{LE}}(t)$ occurs at a certain time $t_{\mathcal{D}^{\text{LE}}}$. A completely analogous situation is possible for the inverse ME, i.e., when $\theta_A^0 < \theta_B^0 < 1$. We will refer to this phenomenon, where $\mathcal{D}_A^{\text{LE}}$ and $\mathcal{D}_B^{\text{LE}}$ intersect but $\theta_A(t)$ and $\theta_B(t)$ do not, as the overshoot ME (OME). This phenomenon is reminiscent of the ME observed in Ref. [21] in supercooled water.

The different scenarios where overshoot-induced humps appear are illustrated in Fig. 9 for direct preparations, i.e., $\theta_A^0 > \theta_B^0 > 1$. In Fig. 9(a), $\theta_A(t)$ and $\theta_B(t)$ do not cross each other, but they both exhibit humps, the one in system B being stronger than in system A. This makes the latter system relax to equilibrium earlier than the former, which physically qualifies as a direct TME. While in the thermal scheme there is no crossing, the positiveness of \mathcal{D}^{LE} forces an intersection between A and B curves, as observed in Fig. 9(b). This is the essence of the OME.

On the other hand, the existence of humps or of a finite crossover time t_θ does not ensure the existence of TME. In fact, in Fig. 9(c) there is a crossing between the thermal curves, but the overshoot-induced humps make the initially hotter system relax later to the equilibrium state, thus frustrating the TME. This is signaled by a

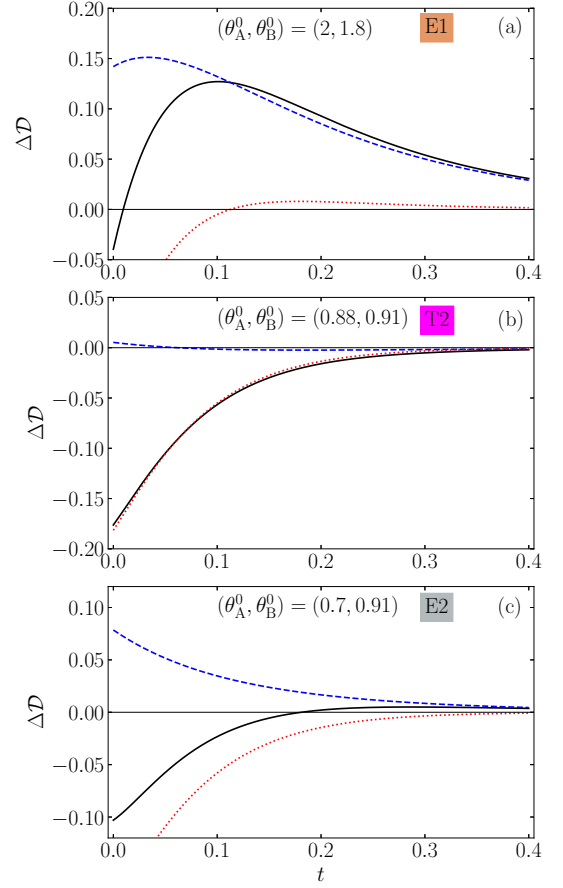


FIG. 8. Same as in Fig. 5, but now for the representative initial condition IV in Table II, $(a_{2A}^0, a_{2B}^0) = (-0.20, 0.50)$. Here, initial temperatures are: (a) $(\theta_B^0 - 1, \theta_A^0 - \theta_B^0) = (0.8, 0.2)$, (b) $(\theta_B^0 - 1, \theta_A^0 - \theta_B^0) = (-0.09, -0.03)$, and (c) $(\theta_B^0 - 1, \theta_A^0 - \theta_B^0) = (-0.09, -0.21)$. Panels (a), (b), and (c) represent examples of cases E1, T2, and E2, respectively [see Fig. 4(d)].

pair of intersections in the \mathcal{D}^{LE} curves of Fig. 9(d), so the OME is absent. The third different scenario is reflected in Figs. 9(e) and 9(f), where there is no crossover either in the thermal evolution or in \mathcal{D}^{LE} , even though sample B exhibits a thermal hump.

The analogous cases for inverse preparations $\theta_A^0 < \theta_B^0 < 1$ are illustrated in Fig. 10.

To summarize, the OME is characterized by a single crossing $\mathcal{D}_A^{\text{LE}} = \mathcal{D}_B^{\text{LE}}$ at a certain time $t_{\mathcal{D}^{\text{LE}}}$, without any crossing between θ_A and θ_B . In order to establish the conditions under which this may happen, let us assume again $|\theta - 1| \ll 1$ and approximate $\ln \theta \approx \theta - 1 - \frac{1}{2}(\theta - 1)^2$ in Eq. (12b). Therefore, the condition $\mathcal{D}_A^{\text{LE}}(t_{\mathcal{D}^{\text{LE}}}) = \mathcal{D}_B^{\text{LE}}(t_{\mathcal{D}^{\text{LE}}})$ with $\theta_A(t_{\mathcal{D}^{\text{LE}}}) \neq \theta_B(t_{\mathcal{D}^{\text{LE}}})$ translates into

$$\theta_A(t_{\mathcal{D}^{\text{LE}}}) - 1 = 1 - \theta_B(t_{\mathcal{D}^{\text{LE}}}). \quad (34)$$

Making use of Eq. (30a) entails

$$t_{\mathcal{D}^{\text{LE}}} = \frac{1}{\lambda_+ - \lambda_-} \ln \left(1 + \frac{\bar{A}_{11}^{-1}}{R_{\text{max}}^0 / R_+^0 - 1} \right), \quad (35)$$

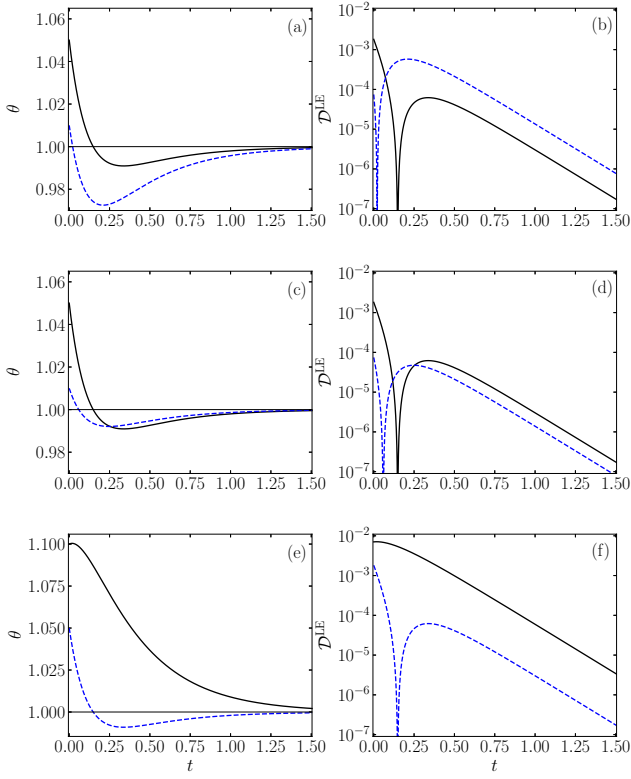


FIG. 9. Time evolution of the temperature and LE relative entropy of samples A and B for the direct case, $\theta_A^0 > \theta_B^0 > 1$. Specifically, we show $\{\theta_A, \mathcal{D}_A^{\text{LE}}\}$ (solid lines) and $\{\theta_B, \mathcal{D}_B^{\text{LE}}\}$ (dashed lines), as obtained from Eq. (30a). Initial conditions are [(a) and (b)] $(\theta_A^0, \theta_B^0) = (1.05, 1.01)$ and $(a_{2A}^0, a_{2B}^0) = (0.5, 0.5)$, [(c) and (d)] $(\theta_A^0, \theta_B^0) = (1.05, 1.01)$ and $(a_{2A}^0, a_{2B}^0) = (0.5, 0.2)$, and [(e) and (f)] $(\theta_A^0, \theta_B^0) = (1.1, 1.05)$ and $(a_{2A}^0, a_{2B}^0) = (-0.35, 0.5)$. In all cases, $\zeta_0 = 1$, $\gamma = 0.1$, and $d = 3$.

where \bar{R}_{max}^0 is defined in Eq. (32) and

$$R_+^0 \equiv \frac{\theta_A^0 + \theta_B^0 - 2}{a_{2A}^0 + a_{2B}^0}. \quad (36)$$

Note the difference between this parameter R_+^0 and the parameter R^0 defined before in Eq. (27). Since $t_{\mathcal{D}^{\text{LE}}}$ must be finite in the OME, the corresponding condition on the initial preparation is

$$0 < R_+^0 < \bar{R}_{\text{max}}^0, \quad (37a)$$

$$R^0 < 0 \text{ or } R^0 > \bar{R}_{\text{max}}^0. \quad (37b)$$

The supplementary condition (37b) represents the violation of Eq. (28) (with $\theta_r \rightarrow 1$) and is needed to exclude any thermal crossing.

According to Eq. (33), if both systems A and B exhibit overshoot-induced humps, the condition given by Eq. (37a) is ensured. As a test, note that $R_{\text{max}}^0 = 0.172$ for all the cases considered in Figs. 9 and 10. The

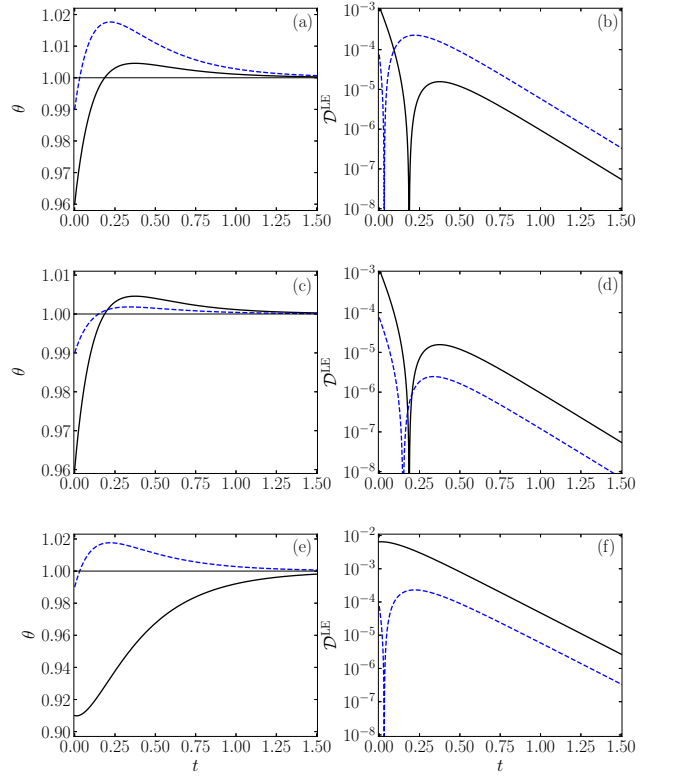


FIG. 10. Same as in Fig. 9, but now for the inverse case $\theta_A^0 < \theta_B^0 < 1$. Initial conditions are [(a) and (b)] $(\theta_A^0, \theta_B^0) = (0.96, 0.99)$ and $(a_{2A}^0, a_{2B}^0) = (-0.35, -0.35)$, [(c) and (d)] $(\theta_A^0, \theta_B^0) = (0.96, 0.99)$ and $(a_{2A}^0, a_{2B}^0) = (-0.35, -0.1)$, and [(e) and (f)] $(\theta_A^0, \theta_B^0) = (0.91, 0.99)$ and $(a_{2A}^0, a_{2B}^0) = (0.3, -0.35)$.

values of (R_+^0, R^0) are $(0.060, \infty)$, $(0.086, 0.133)$, and $(1, -0.059)$ in the cases represented in Figs. 9(a) and 9(b), Figs. 9(c) and 9(d), and Figs. 9(e) and 9(f), respectively. Analogously, (R_+^0, R^0) are $(0.071, \infty)$, $(0.111, 0.120)$, and $(2, -0.123)$ in the cases represented in Figs. 10(a) and 10(b), Figs. 10(c) and 10(d), and Figs. 10(e) and 10(f), respectively. Thus, the OME double condition (37) is fulfilled only in the cases (a) and (b) of Figs. 9 and 10.

VI. SIMULATION RESULTS

In this section, our simulation results are used to test the theoretical predictions stemming from the numerical solutions of: (i) the (nonlinear) BSA, Eqs. (17) and (19a) with $a_3 \rightarrow 0$, and ESA, Eqs. (17) and (19). The theoretical results for the KLD $\mathcal{D}(t)$ and $\mathcal{D}^{\text{LE}}(t)$ are constructed by introducing the theoretical $\theta(t)$ and $a_2(t)$ in Eqs. (12b) and (23), respectively.

The employed computer simulation schemes, DSMC and EDMD, to build the simulation curves are presented in Appendix D. In all cases, the (reduced) initial VDF has been taken as the gamma distribution given by Eq. (21) with the chosen value of the initial excess kurtosis a_2^0 ,

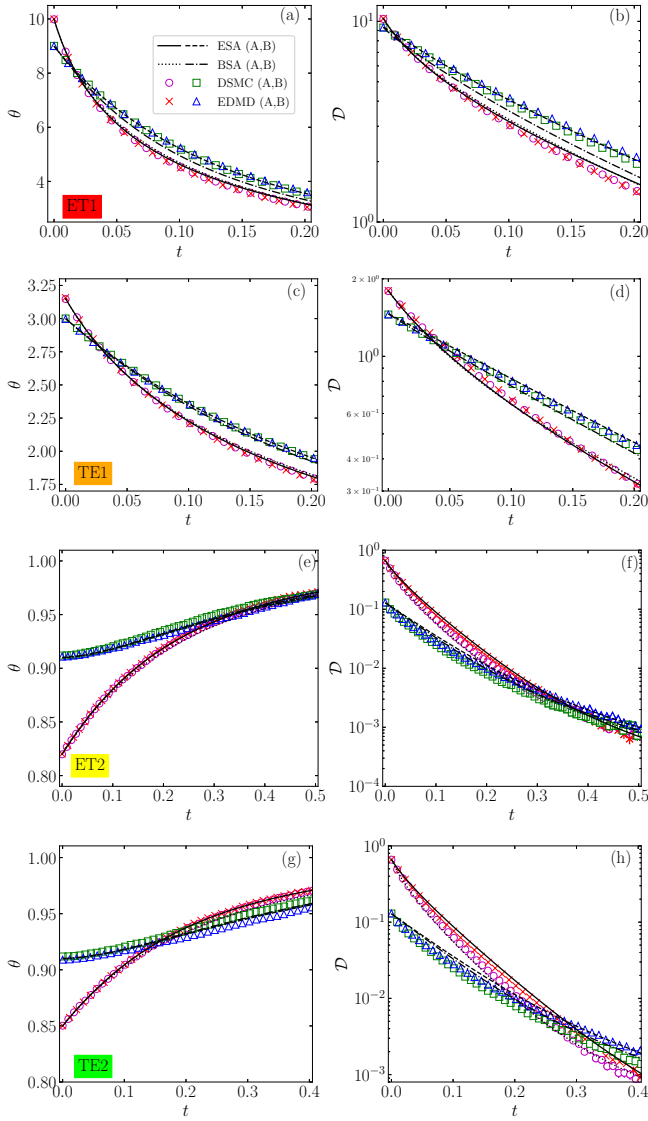


FIG. 11. ME for cases when $\theta - 1$ does not change its sign. Specifically, we plot the time evolution of the temperature and relative entropy for samples A and B: $\{\theta_A, \mathcal{D}_A\}$ (solid and dotted lines, circles, and crosses) and $\{\theta_B, \mathcal{D}_B\}$ (dashed and dash-dotted lines, squares, and triangles). Initial conditions are [(a) and (b)] $(\theta_A^0, \theta_B^0) = (10, 9)$ and $(a_{2A}^0, a_{2B}^0) = (0.5, -0.35)$, [(c) and (d)] $(\theta_A^0, \theta_B^0) = (3.15, 3)$ and $(a_{2A}^0, a_{2B}^0) = (0.5, -0.2)$, [(e) and (f)] $(\theta_A^0, \theta_B^0) = (0.82, 0.91)$ and $(a_{2A}^0, a_{2B}^0) = (-0.35, 0.3)$, and [(g) and (h)] $(\theta_A^0, \theta_B^0) = (0.85, 0.91)$ and $(a_{2A}^0, a_{2B}^0) = (-0.35, 0.3)$. Other parameter values are $\zeta_0 = 1$, $\gamma = 0.1$, and $d = 3$.

as previously done in Refs. [39, 95, 96]. The KLD from simulations is computed as described in Refs. [95, 96].

Figures 11 and 12 contain the theoretical and simulation results of the time evolution of the temperature ratio θ and the KLD \mathcal{D} . The graphs for the cumulants a_2 and a_3 are presented in Appendix E. Samples A and B are prepared with the representative values of the cumulants in Table II, namely pairs I and II (III and IV) for

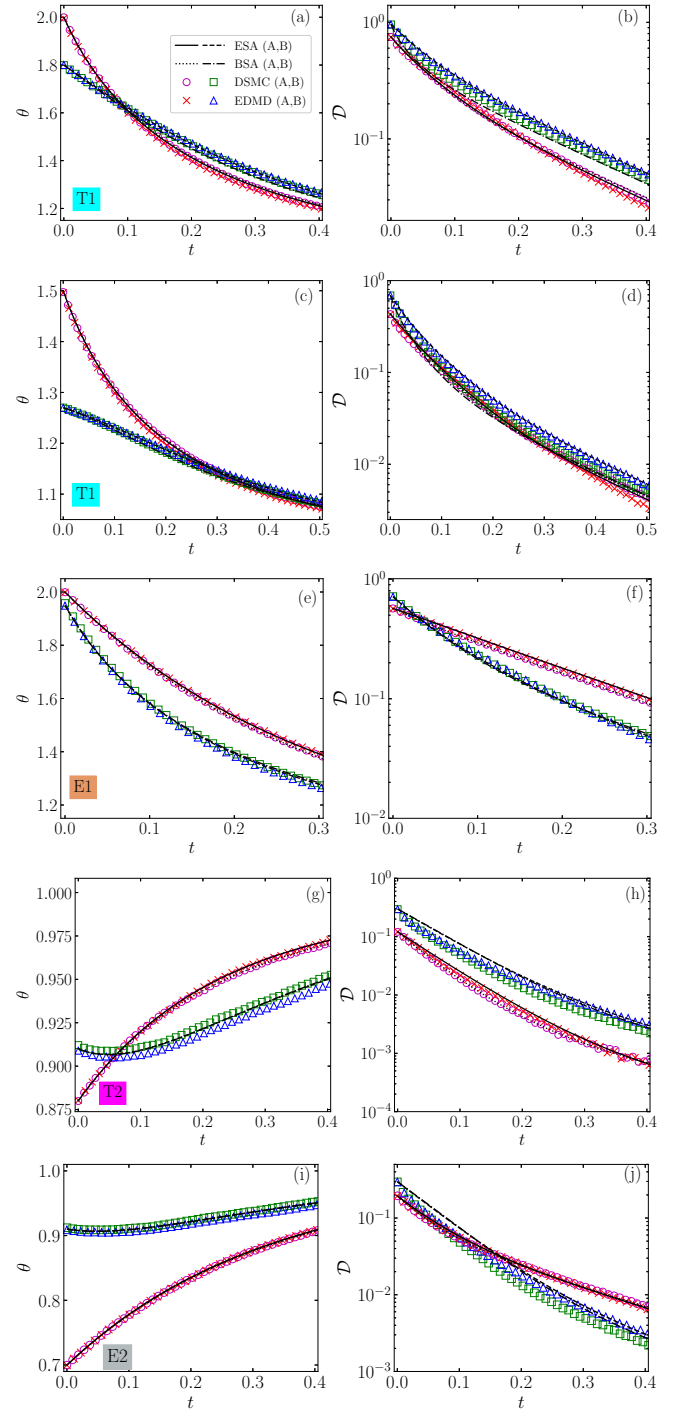


FIG. 12. Same as in Fig. 11, except that the initial conditions are [(a) and (b)] $(\theta_A^0, \theta_B^0) = (2, 1.8)$ and $(a_{2A}^0, a_{2B}^0) = (0.5, -0.35)$, [(c) and (d)] $(\theta_A^0, \theta_B^0) = (1.5, 1.27)$ and $(a_{2A}^0, a_{2B}^0) = (0.5, -0.35)$, [(e) and (f)] $(\theta_A^0, \theta_B^0) = (2, 1.95)$ and $(a_{2A}^0, a_{2B}^0) = (-0.2, 0.5)$, [(g) and (h)] $(\theta_A^0, \theta_B^0) = (0.88, 0.91)$ and $(a_{2A}^0, a_{2B}^0) = (-0.2, 0.5)$, and [(i) and (j)] $(\theta_A^0, \theta_B^0) = (0.7, 0.91)$ and $(a_{2A}^0, a_{2B}^0) = (-0.2, 0.5)$.

the direct (inverse) ME, and different values of the initial temperatures θ_A^0 and θ_B^0 . Pairs (θ_A^0, θ_B^0) are chosen

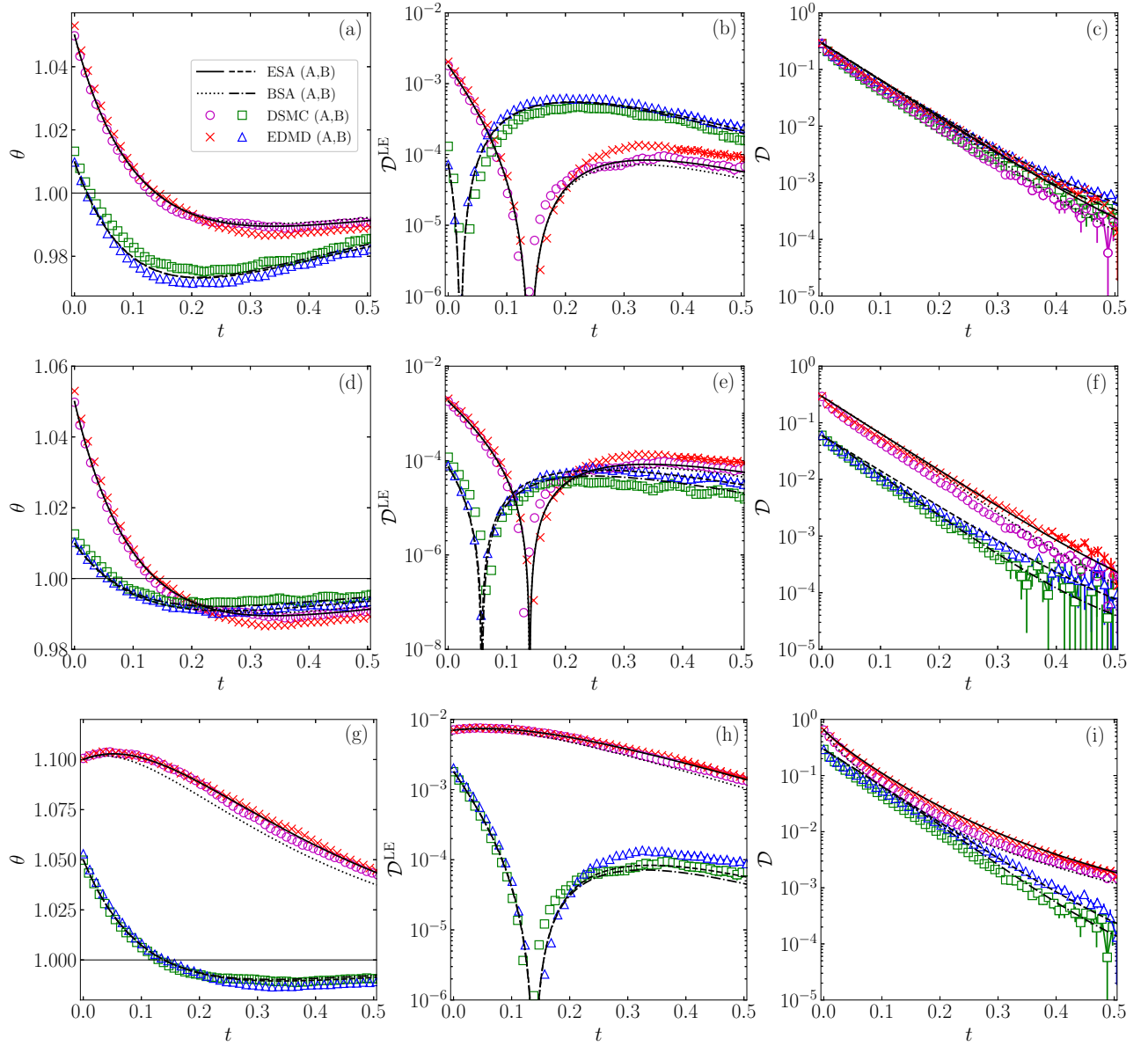


FIG. 13. ME for cases case in which $\theta - 1$ changes sign, i.e., the OME. In this case, we show the time evolution of: $\{\theta_A, \mathcal{D}_A^{\text{LE}}, \mathcal{D}_A\}$ (solid and dotted lines, circles, and crosses) and $\{\theta_B, \mathcal{D}_B^{\text{LE}}, \mathcal{D}_B\}$ (dashed and dash-dotted lines, squares, and triangles). Parameter values and initial conditions correspond to those in Fig. 9.

to illustrate the different cases summarized in Table I. Specifically, we present the cases ET1 in Figs. 11(a) and 11(b), TE1 in Figs. 11(c) and 11(d), ET2 in Figs. 11(e) and 11(f), TE2 in Figs. 11(g) and 11(h), T1 in Figs. 12(a) and 12(b), T1 with a double crossing in \mathcal{D} in Figs. 12(c) and 12(d), E1 in Figs. 12(e) and 12(f), T2 in Figs. 12(g) and 12(h), and E2 in Figs. 12(i) and 12(j). Note that the cases in Figs. 11(a) and 11(b), 11(c) and 11(d), 11(e) and (f), 12(a) and 12(b), 12(g) and 12(h), and 12(i) 12(j) are the same as in Figs. 5(a), 6(b), 7(b), 5(b), 8(b), and 8(c), respectively. Moreover, the case in Figs. 12(c) and 12(d) is close to the case in Fig. 5(c).

It must be remarked that the classification of the case

in Figs. 11(e) and 11(f) as ET2 is less clear than expected. The LBSA theory predicts the ET2 behavior with a wide difference between t_θ and $t_{\mathcal{D}}$, as observed in the inset of Fig. 7(b). Still, nonlinearities reduce the time difference $t_\theta - t_{\mathcal{D}}$. Moreover, the double crossing in \mathcal{D} predicted by the LBSA for the case of Figs. 12(c) and 12(c)(d) is not actually observed in the simulations. The shallow positive maximum of $\mathcal{D}_A - \mathcal{D}_B$ predicted by the LBSA, as seen in Fig. 5(c), is washed out by nonlinear contributions—at least in the case represented in Figs. 12(c) and 12(d).

Let us now turn to the OME predicted by the LBSA, which we have discussed in Sec. V. Figures 13 and 14

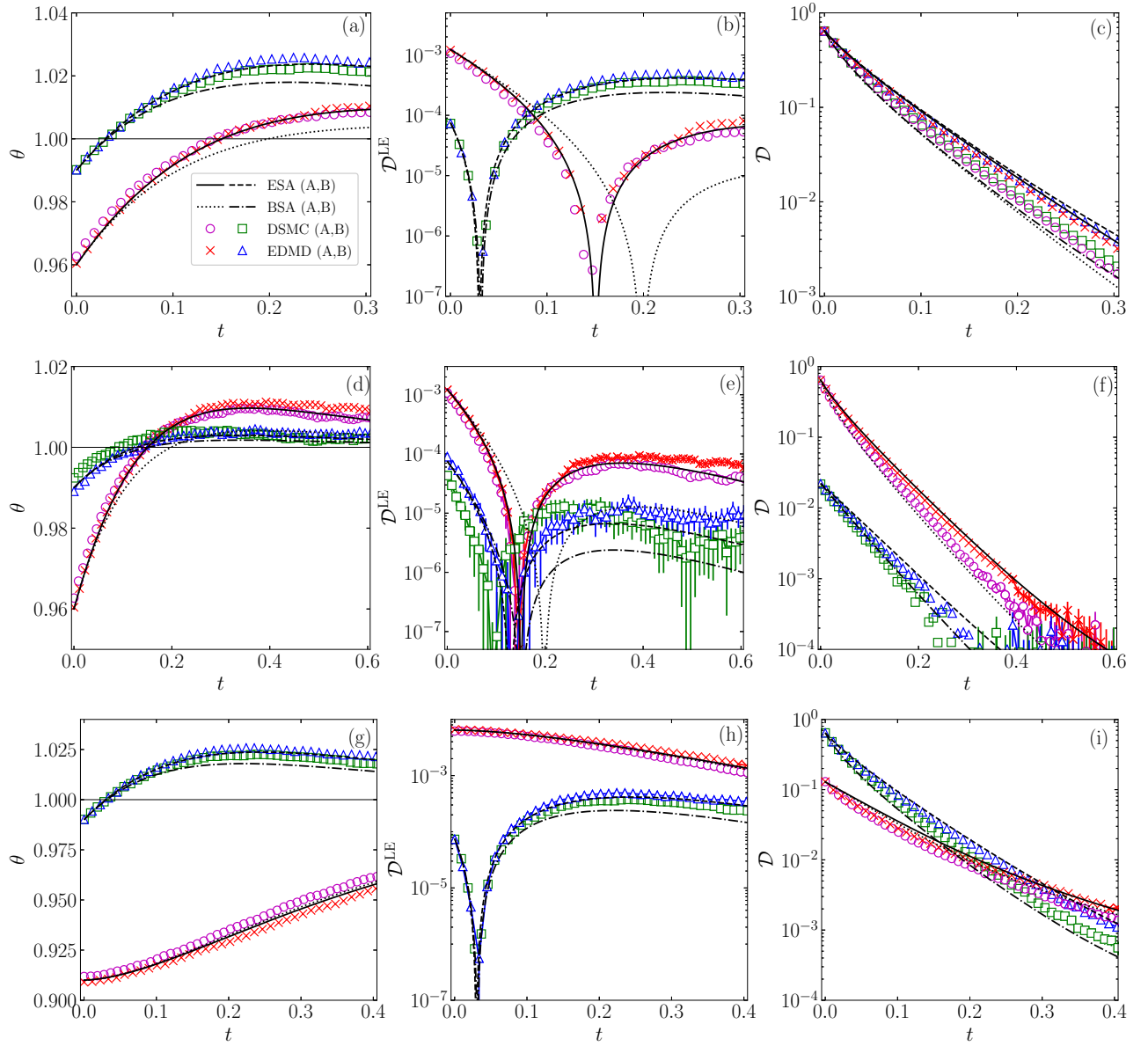


FIG. 14. Same as in Fig. 13, but now for the initial conditions in Fig. 10.

show the time evolution of θ , \mathcal{D}^{LE} , and \mathcal{D} for the same cases as considered in Figs. 9 and 10, respectively. Again, the graphs for a_2 and a_3 can be found in Appendix E. We see that the overshoot behavior and the OME phenomenology are indeed present. The crossover characterizing the TME is accounted for by the intersection of the \mathcal{D}^{LE} curves in Figs. 13(a)–13(c) and 14(a)–14(c), though the corresponding temperature curves never cross.

The figures in this section show that our theoretical predictions for both $\theta(t)$ and $\mathcal{D}(t)$ are generally in very good agreement with DSMC and EDMD simulation results. This is especially true for the ESA, which still gives a good account of the behavior of the fourth cumulant $a_2(t)$ and a fair account of the behavior of the sixth cumulant $a_3(t)$ (see Figs. 17–20), consistently with the results

reported in Ref. [37]. The improvement of the ESA over the BSA can be understood by noticing that the values of the cumulant a_3 are typically of the same magnitude as those of a_2 . It is also worth highlighting the generally good agreement between the simulation results for the relative entropy \mathcal{D} and those obtained from Eqs. (12b) and (23) when θ and a_2 are given by either the BSA or the ESA. This means that the gamma distribution in Eq. (21) represents a convenient proxy of the unknown time-dependent VDF. This ansatz is further confirmed by the generally fair agreement (not shown) between the simulation data for a_3 and the right-hand side of Eq. (22) when plugging the simulation data of a_2 , especially in the cases with $a_2 < 0$.

Finally, we note that small deviations between EDMD

and DSMC simulation are observed (especially for the subtler quantities \mathcal{D} and a_3), despite the low density of the systems. This might be a consequence of the approximations carried out in the numerical implementation of the Langevin dynamics in the *approximate Green function* (AGF) algorithm explained in Appendix D 2. Nevertheless, there is a good agreement for the collisional scheme, as tested in Appendix D 3.

VII. CONCLUSIONS

In this paper, we have analyzed in depth the relaxation to equilibrium of a dilute gas of elastic hard spheres subjected to a nonlinear drag and the associated stochastic force. We have particularly focused on two versions of the ME, namely, the TME and the EME. Our analysis combines theory and simulation. The theoretical approach is based on a Sonine expansion of the solution of the EFPE, Eq. (3). The simulation approach comprises both DSMC results, which integrate numerically Eq. (3), and EDMD results.

We have employed the Kullback–Leibler divergence (or relative entropy) \mathcal{D} , defined in Eq. (9), to measure the distance to equilibrium and monitor the possible emergence of the EME. It must be remarked that other distances to equilibrium have been employed in the literature, as long as they share some common properties of monotonicity, convexity, etc. However, the choice of the distance function does not impinge on the existence of the EME—for a thorough discussion of this issue, see Ref. [51]. The KLD choice for the distance function is quite natural due, to its connection to the nonequilibrium entropy, and especially convenient for comparing the TME and EME, since \mathcal{D} can be decomposed into two summands, see Eqs. (11) and (12). First, the hydrodynamic LE contribution \mathcal{D}^{LE} , which only depends on the temperature and, second, the kinetic-stage correction \mathcal{D}^{kin} , which depends on the whole VDF. To obtain an approximate expression for the latter within the Sonine approximation, we have employed the gamma distribution function, Eq. (23).

For given values of the drag force, i.e., given values of (ζ_0, γ) , the emergence of ME—either direct or inverse—depends on the initial preparations of the two samples (A, whose initial temperature is farther from equilibrium, and B, whose initial temperature is closer to equilibrium). The simplest approach, based on heuristic arguments, is the LBSA given by Eqs. (25). Therein, both the temperature ratio $\theta(t)$ and the excess kurtosis $a_2(t)$ are a linear superposition of two exponentials.

When the difference $\theta - 1$ keeps its initial sign during the relaxation process—i.e., when the temperature does not cross its equilibrium value at a finite time, we have the most usual, standard situation. Bringing to bear that the kinetic-stage contribution \mathcal{D}^{kin} is expected to decay to zero over a shorter timescale than that of the local equilibrium contribution \mathcal{D}^{LE} , we have argued that the

existence of TME implies that of EME (and vice versa) if $\mathcal{D}_A^0 > \mathcal{D}_B^0$. There are two possibilities: either the thermal crossover occurs earlier than the entropic one (scenarios TE1 and TE2 for direct and inverse effects, respectively) or it occurs later than the entropic crossover (scenarios ET1 and ET2 for direct and inverse effects, respectively).

Interestingly, even though θ_A^0 departs from the equilibrium value 1 more than θ_B^0 , one may have $\mathcal{D}_A^0 < \mathcal{D}_B^0$ due to the kinetic contribution \mathcal{D}^{kin} to the entropic distance. This gives rise to the existence of TME without entropy crossover (scenarios T1 and T2 for direct and inverse effects, respectively) or, reciprocally, the existence of EME without thermal crossover (scenarios E1 and E2 for direct and inverse effects, respectively).

A summary of all the possible scenarios above (assuming a constant sign of $\theta - 1$) is provided by Table I. The corresponding phase diagrams in the plane $\theta_A^0 - \theta_B^0$ vs $\theta_B^0 - 1$ are depicted in Fig. 4 for a few representative choices of the initial excess kurtoses a_{2A}^0 and a_{2B}^0 , given in Table II. Those scenarios are modified when the condition of constant sign of $\theta(t) - 1$ is violated, as explained below.

Nonmonotonic evolutions of θ with a crossing of the equilibrium line $\theta = 1$ induce the appearance of overshoot-induced humps. Sample B may relax to equilibrium later than sample A when the temperature of the former overshoots the equilibrium value, a fact that sample A can take advantage of. Even though $\theta_A(t)$ and $\theta_B(t)$ do not intersect, the corresponding curves of \mathcal{D}^{LE} do intersect. We have termed this class of ME as OME. Simple conditions for its existence, Eqs. (37), have been derived by adapting the LBSA to this situation.

The different scenarios for the ME outlined above for the nonlinear fluid, emerging in the extremely simplistic LBSA, have been tested and confirmed by computer simulations (both DSMC and EDMD). These numerical results have also been compared with the more complex nonlinear BSA and ESA. The inclusion of the additional cumulant a_3 in the set of coupled evolution equations allows the ESA to improve over the BSA. Moreover, DSMC and EDMD results are practically indistinguishable, with small discrepancies that can be traced back to the approximations in the EDMD scheme during the free streaming stage, see Appendix D 2. On the other hand, the collisional schemes are tested in Appendix D 3, with good results.

The ME effect is brought about by the nonlinearity in the drag force, which makes the time-evolution of the kinetic temperature be coupled to that of higher cumulants—specifically, to that of the excess kurtosis a_2 for the quadratic dependence of the drag coefficient in Eq. (7). The nonlinear drag force is also responsible for the algebraic nonexponential relaxation after a temperature quench and for the emergence of Kovacs-like response [37]. It is important to remark that these behaviors, and also the ME, survive in the limit $\zeta_0^* \rightarrow \infty$, in which the EFPE reduces to the Fokker–Planck equation—which, interestingly, successfully models mix-

tures of ultracold atoms [75].

The nonmonotonic relaxation of the kinetic temperature observed in the OME entails the necessity of revising the conventional definition of TME. Provided that both initial temperatures are either above (direct case) or below (inverse case) equilibrium, the TME is not necessarily characterized by the crossover of the nonequilibrium temperature but by the crossover of the associated positive-definite quantity \mathcal{D}^{LE} . Within this generalized scheme and for a general complex system, we propose the following, more dependable, definition of the TME based on the idea of local equilibrium: The TME exists in a pair of different initially prepared setups if there are an odd number of crossings between their LE relative entropy \mathcal{D}^{LE} curves. On another note, the definition of the EME is not affected, due to the monotonic decay of the whole relative entropy \mathcal{D} to equilibrium. The EME exists in a pair of samples if their relaxation curves for \mathcal{D} present an odd number of crossings.

It is relevant to stress that the splitting of \mathcal{D} into “kinetic” and “local-equilibrium” contributions can be done on quite a general basis, not only for the molecular fluid we are analyzing in this paper. Moreover, this allows for defining a nonequilibrium temperature $T(t)$, even in systems for which the kinetic temperature makes no sense. Let us consider a general system with Hamiltonian $H(\mathbf{x})$, in which $\mathcal{D}(t)$ is given by Eq. (2). The system is initially prepared in a certain state with average energy $\langle H \rangle^0$ and is put in contact with a thermal bath at temperature T_b . Thus the probability distribution function $P(\mathbf{x}, t)$ relaxes toward the equilibrium distribution $P^{\text{eq}}(\mathbf{x}) = \exp[-H(\mathbf{x})/k_B T_b] / Z(T_b)$, where $Z(T_b)$ is the partition function. One can always introduce a LE distribution with the canonical form $P^{\text{LE}}(\mathbf{x}, T(t)) \equiv \exp[-H(\mathbf{x})/k_B T(t)] / Z(T(t))$, with $T(t)$ being determined self-consistently by the condition

$$\langle H \rangle(t) = \int d\mathbf{x} H(\mathbf{x}) P(\mathbf{x}, t) = \int d\mathbf{x} H(\mathbf{x}) P^{\text{LE}}(\mathbf{x}, T(t)). \quad (38)$$

In this way, $T(t)$ corresponds to the temperature that a system would have at equilibrium if it had an average energy equal to the instantaneous value $\langle H \rangle(t)$. With such a definition of the nonequilibrium temperature $T(t)$, it is easily shown that

$$\mathcal{D}(t) = \mathcal{D}^{\text{kin}}(t) + \mathcal{D}^{\text{LE}}(T(t)), \quad (39)$$

where \mathcal{D}^{kin} and \mathcal{D}^{LE} are given by

$$\mathcal{D}^{\text{kin}}(t) = \int d\mathbf{x} P(\mathbf{x}, t) \ln \frac{P(\mathbf{x}, t)}{P^{\text{LE}}(\mathbf{x}, T(t))}, \quad (40a)$$

$$\mathcal{D}^{\text{LE}}(T(t)) = \int d\mathbf{x} P^{\text{LE}}(\mathbf{x}, T(t)) \ln \frac{P^{\text{LE}}(\mathbf{x}, T(t))}{P^{\text{eq}}(\mathbf{x})}. \quad (40b)$$

Note that $T(t)$ may in general overshoot its equilibrium value T_b , leading to an OME, but \mathcal{D}^{LE} is positive definite and makes it possible to introduce the more reliable definition of the TME explained in the previous paragraph [97].

We expect this work can motivate the experimental investigation, making use of a suitable aging protocol to prepare the initial samples, of the whole variety of ME phenomenology described in this work. Specifically, our predicting and observing the OME—as a novel unexpected behavior—in this molecular gas driven by a nonlinear drag opens the door to its finding in other complex systems. Also, we plan to employ the theoretical and computational framework developed here to study the relaxation times of pairs of temperature quenches thermodynamically equidistant from equilibrium [98, 99], one above and the other one below.

ACKNOWLEDGMENTS

A.M. and A.S. acknowledge financial support from Grant No. PID2020-112936GB-I00 funded by MCIN/AEI/10.13039/501100011033, and from Grants No. IB20079 and No. GR21014 funded by Junta de Extremadura (Spain) and by ERDF “A way of making Europe.” A.P. acknowledges financial support from Grant No. PGC2018-093998-B-I00 funded by MCIN/AEI/10.13039/501100011033/ and by ERDF “A way of making Europe.” A.M. is grateful to the Spanish Ministerio de Ciencia, Innovación y Universidades for a predoctoral fellowship FPU2018-3503. We are grateful to the computing facilities of the Instituto de Computación Científica Avanzada of the University of Extremadura (ICCAEx), where our simulations were run.

Appendix A: Langevin Equation under Nonlinear Drag

In this Appendix, we discuss the Langevin equation associated with the left-hand side of Eq. (3), since the effect of interparticle collisions represented by the right-hand side is well known.

Let us start writing the Langevin equation as

$$\dot{\mathbf{v}}(t) = -\zeta(v(t))\mathbf{v}_i(t) + \xi(v(t))\boldsymbol{\eta}(t), \quad (A1)$$

where $\boldsymbol{\eta}(t)$ is a Gaussian white-noise stochastic term with the statistical properties

$$\langle \boldsymbol{\eta}(t) \rangle_{\text{noise}} = 0, \quad \langle \boldsymbol{\eta}(t)\boldsymbol{\eta}(t') \rangle_{\text{noise}} = \mathbf{l}\delta(t-t'), \quad (A2)$$

where \mathbf{l} is the $d \times d$ unit tensor and $\langle \cdot \rangle_{\text{noise}}$ reads for an average over different realizations. Let us define a Wiener process $W(t)$ with elemental increment $dW(t) = \xi(v(t))\boldsymbol{\eta}(t)dt$. This is the case of a multiplicative noise and, therefore, there is no a unique way of interpreting the proper time within a given interval $[t, t+h]$ at which the process $W(t)$ must be evaluated [100]. In general, one can choose a time $t + \epsilon h$ parameterized by $0 \leq \epsilon \leq 1$.

Hence, the associated Fokker–Planck equation is [100]

$$\partial_t f(\mathbf{v}) - \frac{\partial}{\partial \mathbf{v}} \cdot \left[\zeta(v) \mathbf{v} + \frac{\xi^{2\epsilon}(v)}{2} \frac{\partial}{\partial \mathbf{v}} \xi^{2(1-\epsilon)}(v) \right] f(\mathbf{v}) = 0. \quad (\text{A3})$$

The specific choices $\epsilon = 0$, $\frac{1}{2}$, and 1 correspond to the Itô [67], Stratonovich [67], and Klimontovich [101] interpretations, respectively.

The (differential) fluctuation-dissipation relation stemming from Eq. (A3) turns out to be

$$\zeta(v) = \frac{m\xi^2(v)}{2k_B T_b} - \frac{1-\epsilon}{2v} \frac{\partial \xi^2(v)}{\partial v}. \quad (\text{A4})$$

Only in the Klimontovich interpretation ($\epsilon = 1$) does one recover the conventional fluctuation-dissipation relation, Eq. (5), holding for constant drag coefficient and additive noise. In that case, the left-hand sides of Eqs. (3) and (A3) coincide.

On the other hand, from a simulation point of view, the Itô interpretation ($\epsilon = 0$) is the simplest one to implement. Fortunately, even if $\epsilon \neq 0$ (as happens in the Stratonovich and Klimontovich interpretations), one can always apply the Itô interpretation to the Langevin equation, provided that the original drag coefficient $\zeta(v)$ is replaced by an effective one ζ_{eff} (“spurious drift”). Note first the mathematical identity

$$\xi^{2\epsilon}(v) \frac{\partial}{\partial \mathbf{v}} \xi^{2(1-\epsilon)}(v) f(\mathbf{v}) = \frac{\partial}{\partial \mathbf{v}} \xi^2(v) f(\mathbf{v}) - \epsilon \frac{\partial \xi^2(v)}{\partial v} f(\mathbf{v}). \quad (\text{A5})$$

Inserting this into Eq. (A3), one gets

$$\partial_t f(\mathbf{v}) - \frac{\partial}{\partial \mathbf{v}} \cdot \left[\zeta_{\text{eff}}(v) \mathbf{v} + \frac{\partial \xi^2(v)}{\partial \mathbf{v}} \frac{\xi^2(v)}{2} \right] f(\mathbf{v}) = 0, \quad (\text{A6})$$

where

$$\begin{aligned} \zeta_{\text{eff}}(v) &\equiv \zeta(v) - \frac{\epsilon}{2v} \frac{\partial \xi^2(v)}{\partial v} \\ &= \frac{m\xi^2(v)}{2k_B T_b} - \frac{1}{2v} \frac{\partial \xi^2(v)}{\partial v}. \end{aligned} \quad (\text{A7})$$

In the particular case of Eq. (7) and $\epsilon = 1$, the effective drag coefficient becomes

$$\zeta_{\text{eff}}(v) = \zeta(v) - 2\zeta_0\gamma. \quad (\text{A8})$$

Thus, the original Langevin equation, Eq. (A1), in the Klimontovich interpretation is equivalent to the Langevin equation

$$\dot{\mathbf{v}}(t) = -\zeta_{\text{eff}}(v(t)) \mathbf{v}(t) + \xi(v(t)) \boldsymbol{\eta}(t) \quad (\text{A9})$$

in the Itô interpretation.

Appendix B: Derivation of the evolution equations

To write the hierarchy of moment equations, it is convenient to introduce dimensionless quantities [36]. First,

we define a rescaled velocity \mathbf{c} as

$$\mathbf{c} \equiv \frac{\mathbf{v}}{v_{\text{th}}(t)}, \quad v_{\text{th}}(t) \equiv \sqrt{\frac{2k_B T(t)}{m}}, \quad (\text{B1})$$

in which $v_{\text{th}}(t)$ is the thermal velocity at time t . Analogously, the dimensionless VDF is introduced as

$$\phi(\mathbf{c}, t) \equiv \frac{v_{\text{th}}^d(t)}{n} f(\mathbf{v}, t). \quad (\text{B2})$$

In terms of these reduced quantities, the EFPE, Eq. (3), can be rewritten as

$$\begin{aligned} \partial_t \phi(\mathbf{c}, t) &= \frac{1}{2\theta} \partial_{\mathbf{c}} \cdot \left[\dot{\theta} \mathbf{c} + \zeta_0 (1 + \gamma\theta c^2) (2\theta \mathbf{c} + \partial_{\mathbf{c}}) \right] \phi(\mathbf{c}, t) \\ &\quad + K_d \sqrt{\theta} I[\mathbf{c}|\phi, \phi], \end{aligned} \quad (\text{B3})$$

where θ is the temperature ratio—as defined in Eq. (12b)—and

$$\begin{aligned} I[\mathbf{c}_1|\phi, \phi] &= \int d\mathbf{c}_2 \int_+ d\hat{\sigma} \mathbf{c}_{12} \cdot \hat{\sigma} \\ &\quad \times [\phi(\mathbf{c}'_1, t) \phi(\mathbf{c}'_2, t) - \phi(\mathbf{c}_1, t) \phi(\mathbf{c}_2, t)] \end{aligned} \quad (\text{B4})$$

is the reduced collision operator with $\mathbf{c}_{12} \equiv \mathbf{c}_1 - \mathbf{c}_2$. In Eq. (B3), and consistently with the main text, dimensionless variables are used—recall that the stars on the dimensionless time t^* and the zero-velocity drag coefficient ζ_0^* are dropped.

Multiplying both sides of Eq. (B3) by c^ℓ and defining the reduced moments

$$M_\ell(t) \equiv \langle c^\ell \rangle = \int d\mathbf{c} c^\ell \phi(\mathbf{c}, t), \quad (\text{B5})$$

one obtains the hierarchy of equations [36]

$$\begin{aligned} \frac{\dot{M}_\ell}{\zeta_0} &= \ell \left\{ \left[(\ell - 2)\gamma + (d + 2)\gamma\theta(1 + a_2) - \frac{1}{\theta} \right] M_\ell \right. \\ &\quad \left. - 2\gamma\theta M_{\ell+2} + \frac{d + \ell - 2}{2} \frac{M_{\ell-2}}{\theta} \right\} - \frac{K_d}{\zeta_0} \sqrt{\theta} \mu_\ell, \end{aligned} \quad (\text{B6})$$

where we have introduced the collisional moments μ_ℓ as

$$\mu_\ell \equiv - \int d\mathbf{c} c^\ell I[\mathbf{c}|\phi, \phi]. \quad (\text{B7})$$

Note that $M_0 = 1$, $M_2 = \frac{d}{2}$, and $M_4 = \frac{d(d+2)}{4}(1 + a_2)$ [see Eq. (14)]. Conservation of mass and energy imply that $\mu_0 = \mu_2 = 0$, so that Eq. (B6) is obviously consistent with $\dot{M}_0 = \dot{M}_2 = 0$.

Making use of the explicit form of the collision operator, it is possible to express the collisional moments as two-particle averages of the form

$$\mu_\ell = \int d\mathbf{c}_1 \int d\mathbf{c}_2 \phi(\mathbf{c}_1) \phi(\mathbf{c}_2) \Phi_\ell(\mathbf{c}_1, \mathbf{c}_2). \quad (\text{B8})$$

In particular, $\Phi_2 = 0$ and, after some algebra, one gets

$$\Phi_4(\mathbf{c}_1, \mathbf{c}_2) = \frac{2\pi^{\frac{d-1}{2}}}{\Gamma\left(\frac{d+5}{2}\right)} c_{12} [d(\mathbf{C} \cdot \mathbf{c}_{12})^2 - c_{12}^2 C^2], \quad (\text{B9a})$$

$$\Phi_6(\mathbf{c}_1, \mathbf{c}_2) = 3\Phi_4(\mathbf{c}_1, \mathbf{c}_2) \left(C^2 + \frac{c_{12}^2}{4} \right), \quad (\text{B9b})$$

where $\mathbf{C} \equiv \frac{1}{2}(\mathbf{c}_1 + \mathbf{c}_2)$ is the center-of-mass reduced velocity.

1. Sonine approximation

Let us first consider the case of linear drag force, i.e., $\gamma = 0$. In that case, the LE state defined in Eq. (10) is an exact solution of the EFPE, Eq. (3). Equivalently, in reduced variables,

$$\phi^{\text{LE}}(\mathbf{c}) = \pi^{-d/2} e^{-c^2} \implies M_{2k}^{\text{LE}} = \frac{[d + 2(k-1)]!!}{2^k}, \quad (\text{B10})$$

becomes an exact stationary solution to Eqs. (B3) and (B6), because of the properties $I[\mathbf{c}|\phi^{\text{LE}}, \phi^{\text{LE}}] = 0$, $\mu_\ell^{\text{LE}} = 0$. Moreover, the solution to Eq. (17) is simply $\theta(t) = 1 + [\theta(0) - 1]e^{-2\zeta_0 t}$, as stated in the main text. Thus, if $\gamma = 0$ and the system is initially prepared in an equilibrium state with a temperature $T(0)$, its coupling to a bath at temperature T_b makes the temperature evolve toward T_b but otherwise the system remains always in local equilibrium, i.e., the VDF is Maxwellian with the time-dependent temperature.

Going back to the nonlinear case $\gamma \neq 0$, the VDF can be represented by the Sonine expansion

$$\phi(\mathbf{c}; t) = \phi^{\text{LE}}(\mathbf{c}) \left[1 + \sum_{j=2}^{\infty} a_j(t) L_j^{(\frac{d-2}{2})}(c^2) \right], \quad (\text{B11})$$

where $L_j^{(\frac{d-2}{2})}(c^2)$ are generalized Laguerre (or Sonine) polynomials and the coefficients $a_j = [j!\Gamma(\frac{d}{2})/\Gamma(j + \frac{d}{2})] \langle L_j^{(\frac{d-2}{2})}(c^2) \rangle$ are the cumulants of the nonequilibrium VDF. The associated velocity moments are

$$M_{2k} = M_{2k}^{\text{LE}} \left[1 + \sum_{j=2}^k (-1)^j \binom{k}{j} a_j \right], \quad k \geq 2. \quad (\text{B12})$$

In particular,

$$M_6 = \frac{d(d+2)(d+4)}{8} (1 + 3a_2 - a_3), \quad (\text{B13a})$$

$$M_8 = \frac{d(d+2)(d+4)(d+6)}{16} (1 + 6a_2 - 4a_3 + a_4). \quad (\text{B13b})$$

The infinite moment hierarchy, Eq. (B6), cannot be solved in an exact way in general. This is even the case for linear drag, $\gamma = 0$, when the initial state is not a Maxwellian. As a consequence, the exact evolution of the temperature ratio $\theta(t)$ cannot be obtained from Eq. (17) if $\gamma \neq 0$.

Let us suppose, however, that the initial condition and subsequent evolution are sufficiently close to the LE state as to assume both the cumulants in Eq. (B11) beyond a_3 and the quadratic terms in a_2, a_3 (i.e., those proportional to a_2^2, a_3^2 , and $a_2 a_3$) being negligible. In that case, the two first nontrivial collisional moments become [102]

$$\mu_4 \approx \frac{2(d-1)}{K_d} \left(a_2 - \frac{a_3}{4} \right), \quad (\text{B14a})$$

$$\mu_6 \approx \frac{3(d-1)(2d+9)}{2K_d} \left(a_2 - \frac{3a_3}{4} \right). \quad (\text{B14b})$$

Within this scheme, Eq. (B6) with $\ell = 4$ and $\ell = 6$ yields Eq. (19) in the main text.

Appendix C: Parameters in Eqs. (25)

The parameters λ_\pm, B_i , and A_{ij} are given by

$$\lambda_\pm = \frac{\Lambda_{11} + \Lambda_{22} \pm \sqrt{(\Lambda_{11} - \Lambda_{22})^2 + 4\Lambda_{12}\Lambda_{21}}}{2}, \quad (\text{C1a})$$

$$B_1 = \theta_r + \frac{\Lambda_{22}C_1 - \Lambda_{12}C_2}{\Lambda_{11}\Lambda_{22} - \Lambda_{12}\Lambda_{21}}, \quad B_2 = \frac{\Lambda_{11}C_2 - \Lambda_{21}C_1}{\Lambda_{11}\Lambda_{22} - \Lambda_{12}\Lambda_{21}}, \quad (\text{C1b})$$

$$A_{11} = \frac{\lambda_+ - \Lambda_{11}}{\lambda_+ - \lambda_-}, \quad A_{22} = \frac{\lambda_+ - \Lambda_{22}}{\lambda_+ - \lambda_-}, \quad (\text{C1c})$$

$$A_{12} = \frac{\Lambda_{12}}{\lambda_+ - \lambda_-}, \quad A_{21} = \frac{\Lambda_{21}}{\lambda_+ - \lambda_-}, \quad (\text{C1d})$$

where

$$\Lambda_{11} = 2\zeta_0 [1 + (d+2)\gamma(2\theta_r - 1)], \quad (\text{C2a})$$

$$\Lambda_{22} = \zeta_0 \left[\frac{4}{\theta_r} - 8\gamma + 4(d+8)\gamma\theta_r \right] + \frac{8(d-1)}{d(d+2)} \sqrt{\theta_r}, \quad (\text{C2b})$$

$$\Lambda_{12} = 2\zeta_0(d+2)\gamma\theta_r^2, \quad \Lambda_{21} = 8\zeta_0\gamma, \quad (\text{C2c})$$

$$C_1 = 2\zeta_0(1 - \theta_r) [1 + (d+2)\gamma\theta_r], \quad C_2 = 8\zeta_0\gamma(1 - \theta_r). \quad (\text{C2d})$$

Appendix D: Computer Simulation Schemes

We have performed DSMC and EDMD simulations of the model to test the theoretical predictions. In both schemes, the nonlinear drag is implemented at the level of stochastic equations of motion by using Eq. (A9) and applying the associated Wiener process at time t within the interval $[t, t+h]$.

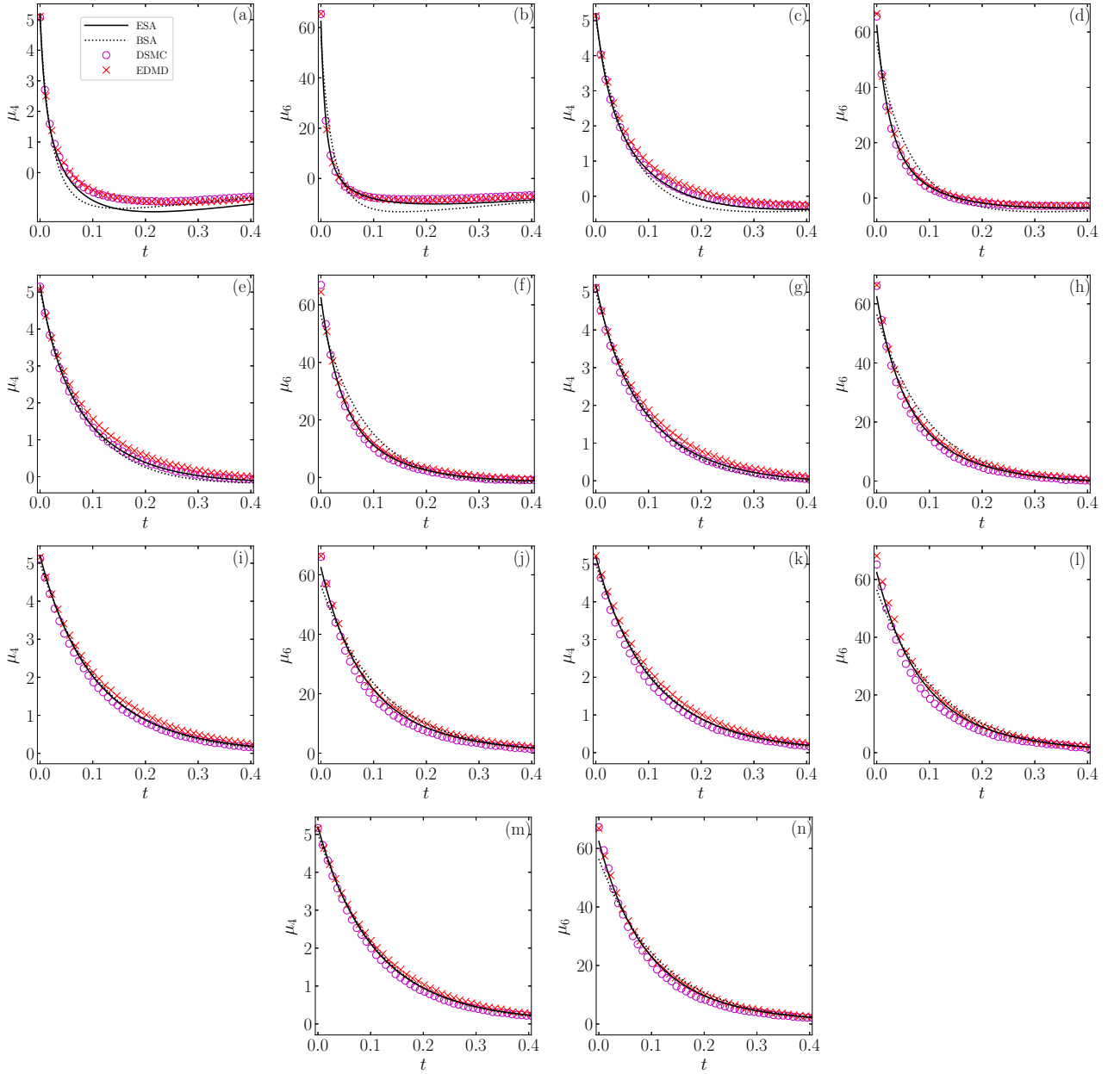


FIG. 15. Evolution of the collisional moments μ_4 and μ_6 for $\zeta_0 = 1$, $\gamma = 0.1$, $d = 3$, and initial conditions $a_2^0 = 0.5$ and [(a) and (b)] $\theta^0 = 10$, [(c) and (d)] $\theta^0 = 3.15$, [(e) and (f)] $\theta^0 = 2$, [(g) and (h)] $\theta^0 = 1.5$, [(i) and (j)] $\theta^0 = 1.05$, [(k) and (l)] $\theta^0 = 1.01$, and [(m) and (n)] $\theta^0 = 0.91$. Symbols correspond to simulation data for DSMC (\circ) and EDMD (\times) schemes, while lines represent the theoretical predictions for ESA (—) and BSA (\cdots).

1. Direct simulation Monte Carlo

The implementation of DSMC for this system is based on the pioneering work by Bird [103, 104], except for our taking into account of both the nonlinear drag and white-noise forces during the free-streaming stage of the algorithm [105].

Let us assume a homogeneous system of N particles, where their dynamics is just controlled by their velocities $\{\mathbf{v}_i\}$ with $i = 1, \dots, N$, and positions are obviated. The

discrete VDF of such a system of particles is given by

$$n^{-1}f(\mathbf{v}, t) = \frac{1}{N} \sum_{i=1}^N \delta(\mathbf{v}_i(t) - \mathbf{v}). \quad (\text{D1})$$

At the initialization of the system, the squared moduli of the particles velocities $\{v_i^2(0)\}$ are drawn from a gamma distribution parameterized by $\langle v^2(0) \rangle = dk_B T^0/m$ and $\langle v^4(0) \rangle = d(d+2)(k_B T^0/m)^2(1+a_2^0)$. Next, the velocity vectors $\{\mathbf{v}_i(0)\}$ are constructed from these moduli, with random directions. To enforce a vanishing initial total

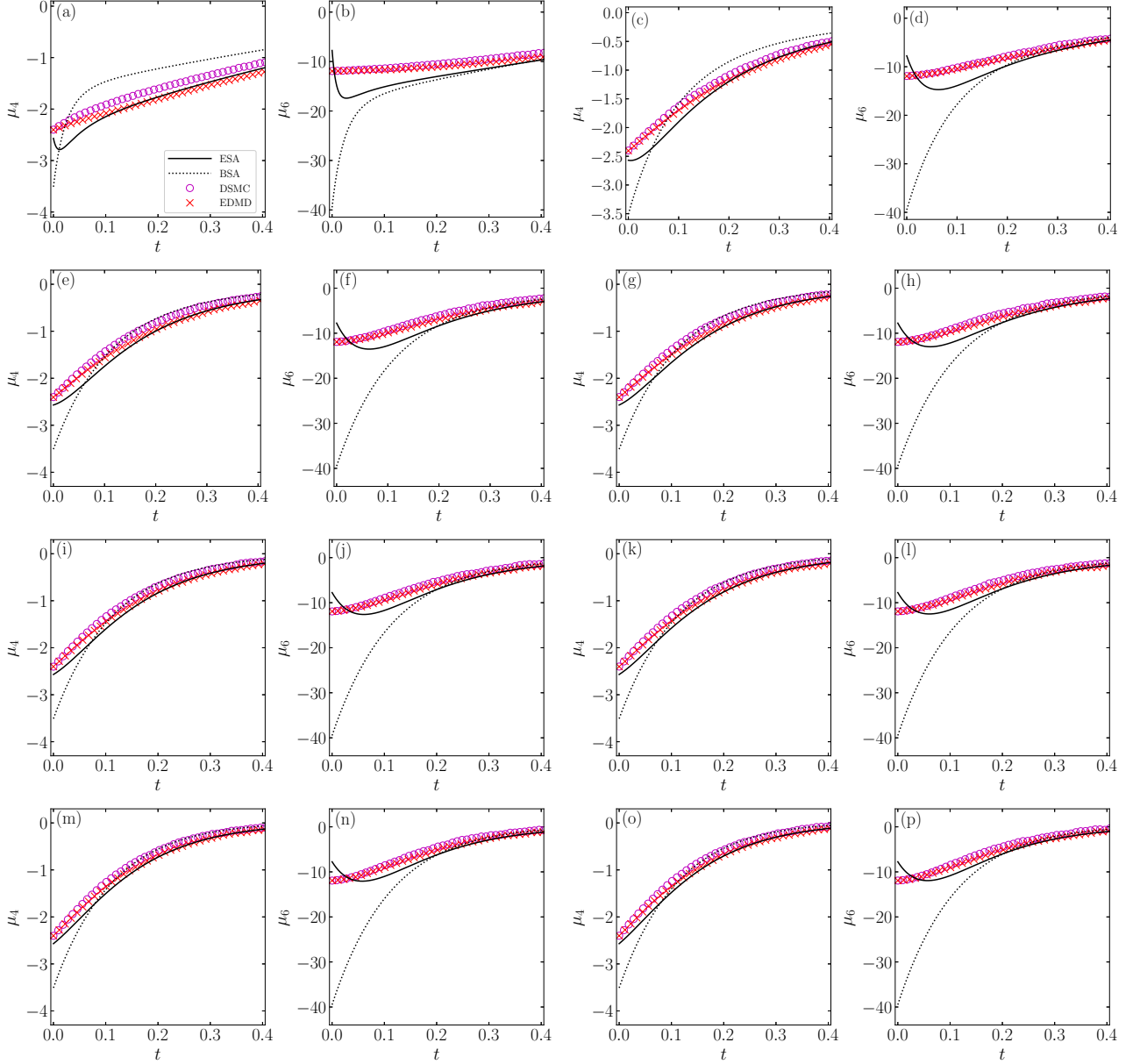


FIG. 16. Evolution of the collisional moments μ_4 and μ_6 for $\zeta_0 = 1$, $\gamma = 0.1$, $d = 3$, and initial conditions $a_2^0 = -0.35$ and [(a) and (b)] $\theta^0 = 9$, [(c) and (d)] $\theta^0 = 1.8$, [(e) and (f)] $\theta^0 = 1.27$, [(g) and (h)] $\theta^0 = 1.1$, and [(i) and (j)] $\theta^0 = 0.99$, [(k) and (l)] $\theta^0 = 0.96$, [(m) and (n)] $\theta^0 = 0.85$, and [(o) and (p)] $\theta^0 = 0.82$. Symbols correspond to simulation data for DSMC (o) and EDMD (x) schemes, while lines represent the theoretical predictions for ESA (—) and BSA (⋯).

momentum, the velocity of every particle is subsequently subtracted by the amount $N^{-1} \sum_i \mathbf{v}_i(0)$.

After initialization, velocities are updated from t to $t+h$ (where the time step h is much smaller than the mean free time) by splitting the algorithm into two different stages: collisions and free streaming.

During the collision stage, a number $\frac{1}{2}N\omega_{\max}h$ of pairs are randomly chosen with uniform probability, where ω_{\max} is an upper bound estimate for the collision rate of one particle. Then, given a pair ij , the collision is accepted (acceptance-rejection Metropolis criterion) with

probability $\Theta(\mathbf{v}_{ij} \cdot \hat{\boldsymbol{\sigma}}_{ij})\omega_{ij}/\omega_{\max}$, where $\hat{\boldsymbol{\sigma}}_{ij}$ a random vector in the unit d -sphere and $\omega_{ij} = \Omega_d \sigma^{d-1} n g_c |\mathbf{v}_{ij} \cdot \hat{\boldsymbol{\sigma}}_{ij}|$ with $\Omega_d = 2\pi^{d/2}/\Gamma(d/2)$ being the d -dimensional solid angle. If the collision is accepted for the given pair, then postcollisional velocities are assigned following the collisional rules for elastic hard spheres, namely $\mathbf{v}_{i,j} \rightarrow \mathbf{v}_{i,j} \mp (\mathbf{v}_{ij} \cdot \hat{\boldsymbol{\sigma}}_{ij})\hat{\boldsymbol{\sigma}}_{ij}$. If $\omega_{ij} > \omega_{\max}$ in one of the sampled pairs, then the collision is accepted and the estimate is updated as $\omega_{\max} = \omega_{ij}$.

During free streaming, velocities are updated accord-

ing to the scheme given by (A9), namely

$$\begin{aligned} \mathbf{v}_i(t) \rightarrow \mathbf{v}_i(t+h) \approx & \mathbf{v}_i(t) - \zeta_{\text{eff}}(v_i(t))\mathbf{v}_i(t)h \\ & + \xi(v_i(t))\sqrt{h}\mathbf{Y}_i + \mathcal{O}(h^{3/2}), \end{aligned} \quad (\text{D2})$$

where \mathbf{Y}_i is a random vector drawn from the Gaussian probability distribution

$$P(\mathbf{Y}) = (2\pi)^{-d/2} e^{-Y^2/2}. \quad (\text{D3})$$

In our DSMC algorithm we took $N = 10^4$ three-dimensional particles ($d = 3$) and chose a time step $h = 10^{-2}\lambda/\sqrt{2k_B T_b/m}$, where $\lambda = (\sqrt{2\pi n}\sigma^2)^{-1}$ is the mean free path.

2. Event-driven molecular dynamics

EDMD algorithms are based on the evolution driven by events which can be particle-particle collisions, boundary effects, or other more complex interactions. Between two consecutive events, there is a free streaming of particles. Again, the stochastic and drag forces directly influence the particle dynamics. Whereas in DSMC positions were not required, in EDMD they are essential and are affected by the nonlinear noise, as explained below.

In order to implement the effect of the Langevin dynamics in our EDMD simulations, we have followed the AGF algorithm proposed in Ref. [106]. Since $\dot{\mathbf{r}}_i(t) = \mathbf{v}(t)$, Eq. (D2) must be supplemented by [106]

$$\begin{aligned} \mathbf{r}_i(t) \rightarrow \mathbf{r}_i(t+h) \approx & \mathbf{r}_i(t) + \mathbf{v}_i(t)h \left[1 - \frac{\zeta_{\text{eff}}(v_i(t))}{2}h \right] \\ & + \frac{1}{2}\xi(v_i(t))h^{3/2}\mathbf{W}_i + \mathcal{O}(h^{5/2}), \end{aligned} \quad (\text{D4})$$

with

$$\mathbf{W}_i = \mathbf{Y}_i + \sqrt{\frac{5}{3}}\bar{\mathbf{Y}}_i, \quad (\text{D5})$$

where we have particularized the algorithm to the three-dimensional geometry, \mathbf{Y}_i is the random vector appearing in Eq. (D2), and $\bar{\mathbf{Y}}_i$ is an independent random vector, also drawn from the Gaussian distribution (D3). Notice that, since the equation for $\mathbf{v}_i(t)$ is expanded up to $\mathcal{O}(h^{3/2})$ and $\mathbf{r}_i(t+h) - \mathbf{r}_i(t) \sim \mathbf{v}_i(t)h$, then the equation for $\mathbf{r}_i(t)$ needs to be expanded up to $\mathcal{O}(h^{5/2})$.

In our EDMD simulations, we deal with a system of $N = 1.065 \times 10^4$ spheres and reduced number density $n\sigma^3 = 10^{-3}$. The time step is $h = 10^{-3}\lambda/\sqrt{2k_B T_b/m}$, and periodic boundary conditions are used.

3. Test of the time evolution of the collisional moments μ_4 and μ_6

Let us present now a comparison between the collisional moments μ_4 and μ_6 measured in simulations and

those provided by the ESA and the BSA. In the ESA, those collisional moments are given by Eqs. (B14), complemented with the numerical solution of Eqs. (17) and (19). Analogously, in the BSA, the collisional moments are given by Eqs. (B14) with $a_3 \rightarrow 0$, complemented with the numerical solution of Eqs. (17) and (19a), again with $a_3 \rightarrow 0$.

In the simulations (both DSMC and EDMD), the following numerical scheme has been used to address the computation of the collisional moments [105, 107]. We randomly choose $N' = 10^6$ pairs of particles out of the total number $N(N-1)/2 = 5 \times 10^7$ and approximate the collisional moments as

$$\mu_\ell = \frac{1}{N'} \sum_{ij}^{N'} \Phi_\ell(\mathbf{c}_i, \mathbf{c}_j), \quad (\text{D6})$$

where Φ_4 and Φ_6 are given by Eqs. (B9).

Figures 15 and 16 show the time evolution of μ_4 and μ_6 , as measured in our DSMC and EDMD simulations and as predicted by the BSA and ESA, for a number of representative initial conditions. A very good agreement between DSMC and EDMD is found; the small differences between them could explain the deviations observed in Figs. 10–12. There is also a general good agreement with the ESA results, while the BSA predictions exhibit important deviations in the initial stage, especially in the case of μ_6 . The deviations of the BSA and ESA are due to the nonnegligible role played by nonlinear terms of the form a_2^2 , a_3^2 , and $a_2 a_3$, as well as by higher-order cumulants. Interestingly, those deviations are more relevant for negative a_2^0 than for positive a_2^0 and tend to increase as the initial temperature θ^0 grows—in accordance with the results in Ref. [37] for a quench to low temperatures.

Appendix E: Evolution of the cumulants a_2 and a_3

In this Appendix we present a comparison between the simulation results for the cumulants a_2 and a_3 , and the theoretical predictions BSA (for a_2 only) and ESA. The results are displayed in Figs. 17–20.

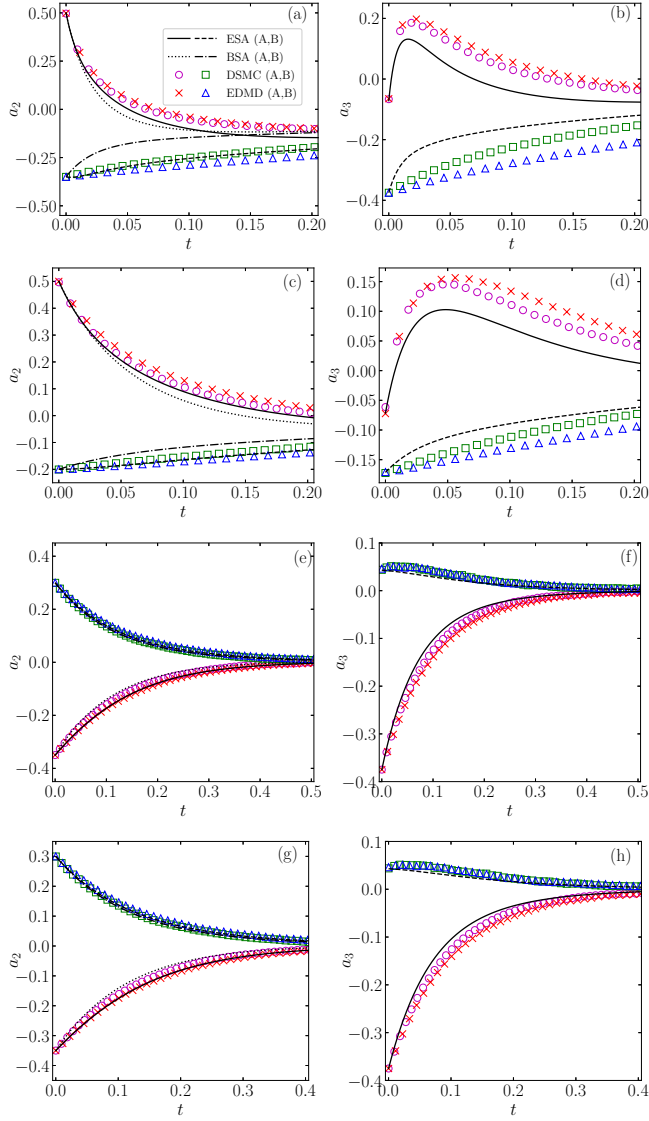


FIG. 17. Same as in Fig. 11, except that the quantities plotted are a_2 and a_3 .

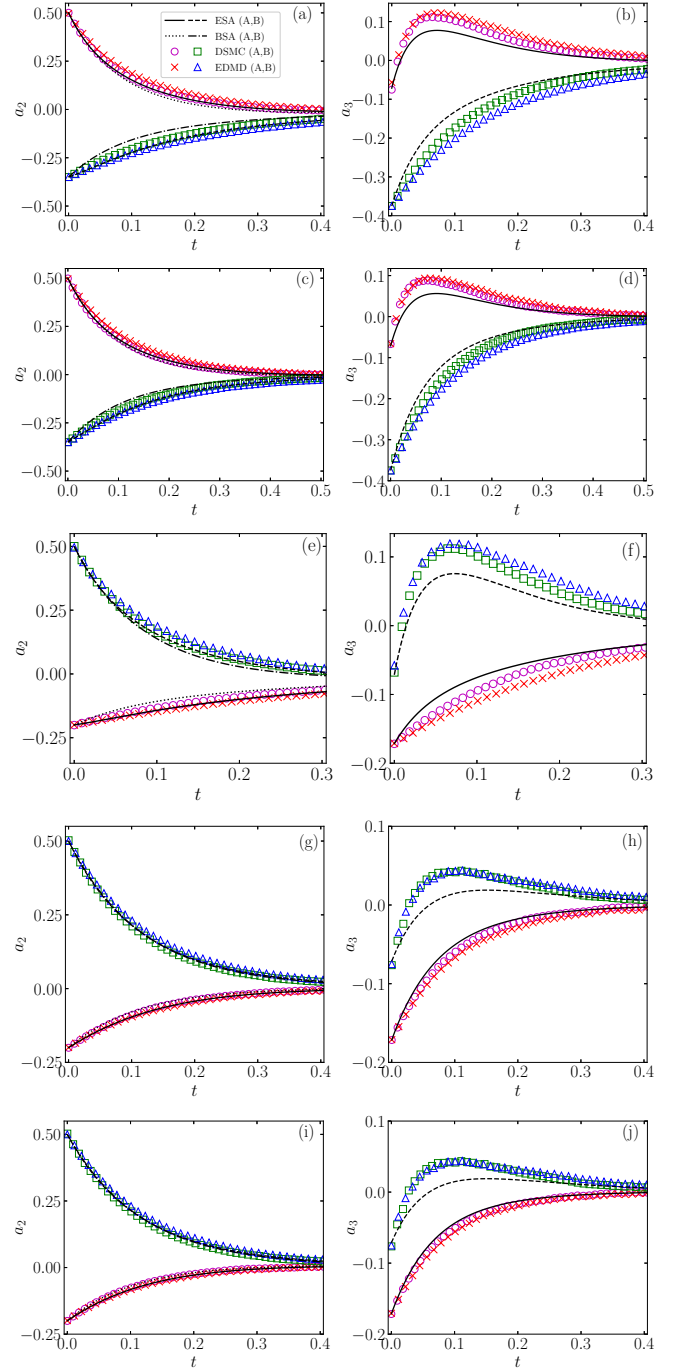


FIG. 18. Same as in Fig. 12, except that the quantities plotted are a_2 and a_3 .

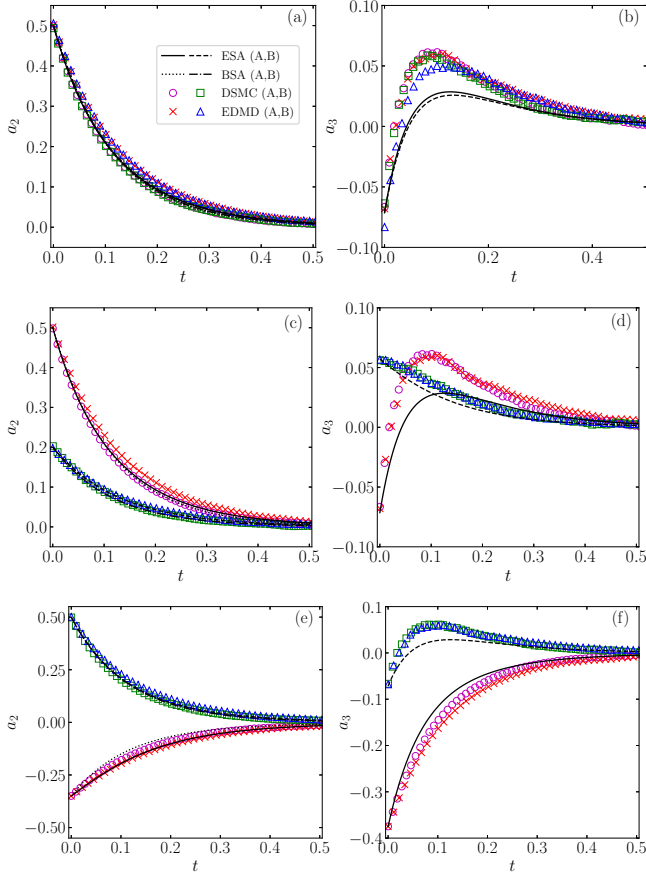


FIG. 19. Same as in Fig. 13, except that the quantities plotted are a_2 and a_3 .

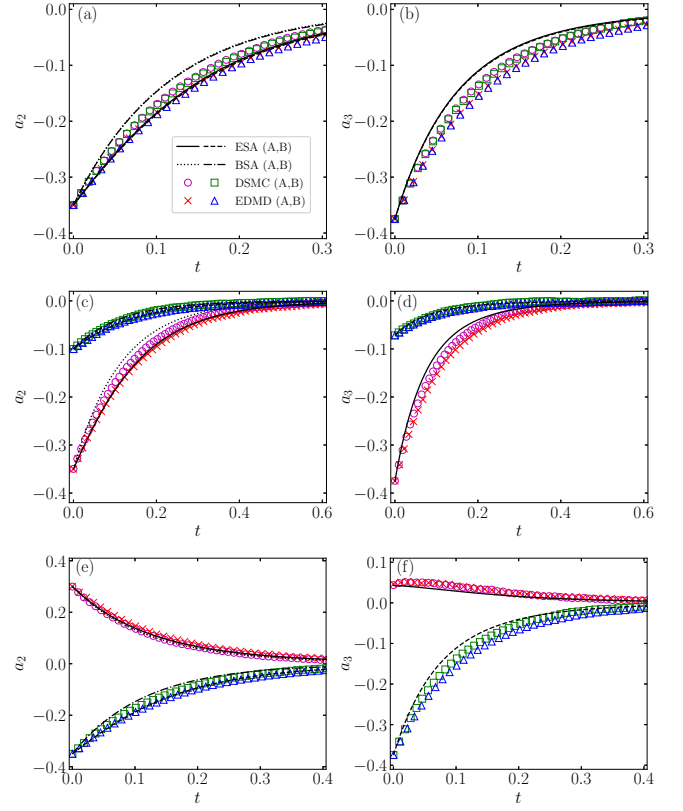


FIG. 20. Same as in Fig. 14, except that the quantities plotted are a_2 and a_3 .

-
- [1] N. C. Keim, J. D. Paulsen, Z. Zeravcic, S. Sastry, and S. R. Nagel, Memory formation in matter, *Rev. Mod. Phys.* **91**, 035002 (2019).
- [2] E. B. Mpemba and D. G. Osborne, Cool?, *Phys. Educ.* **4**, 172 (1969).
- [3] G. S. Kell, The freezing of hot and cold water, *Am. J. Phys.* **37**, 564 (1969).
- [4] I. Firth, Cooler?, *Phys. Educ.* **6**, 32 (1971).
- [5] E. Deeson, Cooler-lower down, *Phys. Educ.* **6**, 42 (1971).
- [6] F. C. Frank, The Descartes–Mpemba phenomenon, *Phys. Educ.* **9**, 284 (1974).
- [7] R. Gallea, The Bacon–Descartes–Mpemba phenomenon, *Phys. Educ.* **9**, 490 (1974).
- [8] J. Walker, Hot water freezes faster than cold water. Why does it do so?, *Sci. Am.* **237**, 246 (1977).
- [9] D. G. Osborne, Mind on ice, *Phys. Educ.* **14**, 414 (1979).
- [10] M. Freeman, Cooler still—an answer?, *Phys. Educ.* **14**, 417 (1979).
- [11] K. Kumar, Mpemba effect and 18th century ice-cream, *Phys. Educ.* **15**, 268 (1980).
- [12] J. W. Hanneken, Mpemba effect and cooling by radiation to the sky, *Phys. Educ.* **16**, 7 (1981).
- [13] B. Wojciechowski, I. Owczarek, and G. Bednarz, Freezing of aqueous solutions containing gases, *Cryst. Res. Technol.* **23**, 843 (1988).
- [14] D. Auerbach, Supercooling and the Mpemba effect: When hot water freezes quicker than cold, *Am. J. Phys.* **63**, 882 (1995).
- [15] C. A. Knight, The Mpemba effect: The freezing times of cold and hot water, *Am. J. Phys.* **64**, 524 (1996).
- [16] P. K. Maciejewski, Evidence of a convective instability allowing warm water to freeze in less time than cold water, *J. Heat Transf.* **118**, 65 (1996).
- [17] M. Jeng, The Mpemba effect: When can hot water freeze faster than cold?, *Am. J. Phys.* **74**, 514 (2006).
- [18] S. Esposito, R. De Risi, and L. Somma, Mpemba effect and phase transitions in the adiabatic cooling of water before freezing, *Physica A* **387**, 757 (2008).
- [19] J. I. Katz, When hot water freezes before cold, *Am. J. Phys.* **77**, 27 (2009).
- [20] M. Vynnycky and S. L. Mitchell, Evaporative cooling and the Mpemba effect, *Heat Mass Transf.* **46**, 881 (2010).
- [21] J. D. Brownridge, When does hot water freeze faster than cold water? A search for the Mpemba effect, *Am. J. Phys.* **79**, 78 (2011).

- [22] M. Vynnycky and N. Maeno, Axisymmetric natural convection-driven evaporation of hot water and the Mpemba effect, *Int. J. Heat Mass Transf.* **55**, 7297 (2012).
- [23] M. Balázovič and B. Tomášik, The Mpemba effect, Shechtman's quasicrystals and student exploration activities, *Phys. Educ.* **47**, 568 (2012).
- [24] X. Zhang, Y. Huang, Z. Ma, Y. Zhou, J. Zhou, W. Zheng, Q. Jiang, and C. Q. Sun, Hydrogen-bond memory and water-skin supersolidity resolving the Mpemba paradox, *Phys. Chem. Chem. Phys.* **16**, 22995 (2014).
- [25] M. Vynnycky and S. Kimura, Can natural convection alone explain the Mpemba effect?, *Int. J. Heat Mass Transf.* **80**, 243 (2015).
- [26] C. Q. Sun, Behind the Mpemba paradox, *Temperature* **2**, 38 (2015).
- [27] M. Balázovič and B. Tomášik, Paradox of temperature decreasing without unique explanation, *Temperature* **2**, 61 (2015).
- [28] A. A. Romanovsky, Which is the correct answer to the Mpemba puzzle?, *Temperature* **2**, 63 (2015).
- [29] J. Jin and W. A. Goddard, Mechanisms underlying the Mpemba effect in water from molecular dynamics simulations, *J. Phys. Chem. C* **119**, 2622 (2015).
- [30] R. T. Ibekwe and J. P. Cullerne, Investigating the Mpemba effect: when hot water freezes faster than cold water, *Phys. Educ.* **51**, 025011 (2016).
- [31] A. Gijón, A. Lasanta, and E. R. Hernández, Paths towards equilibrium in molecular systems: The case of water, *Phys. Rev. E* **100**, 032103 (2019).
- [32] J. Bechhoefer, A. Kumar, and R. Chétrite, A fresh understanding of the Mpemba effect, *Nat. Rev. Phys.* **3**, 534 (2021).
- [33] H. C. Burridge and P. F. Linden, Questioning the Mpemba effect: hot water does not cool more quickly than cold, *Sci. Rep.* **6**, 37665 (2016).
- [34] H. C. Burridge and O. Hallstadius, Observing the Mpemba effect with minimal bias and the value of the Mpemba effect to scientific outreach and engagement, *Proc. R. Soc. A* **476**, 20190829 (2020).
- [35] D. C. Elton and P. D. Spencer, Pathological Water Science — Four Examples and What They Have in Common, in *Biomechanical and Related Systems*, Biologically-Inspired Systems, Vol. 17, edited by A. Gadomski (Springer, Cham., 2021) pp. 155–169.
- [36] A. Santos and A. Prados, Mpemba effect in molecular gases under nonlinear drag, *Phys. Fluids* **32**, 072010 (2020).
- [37] A. Patrón, B. Sánchez-Rey, and A. Prados, Strong non-exponential relaxation and memory effects in a fluid with nonlinear drag, *Phys. Rev. E* **104**, 064127 (2021).
- [38] R. Gómez González, N. Khalil, and V. Garzó, Mpemba-like effect in driven binary mixtures, *Phys. Fluids* **33**, 053301 (2021).
- [39] A. Lasanta, F. Vega Reyes, A. Prados, and A. Santos, When the hotter cools more quickly: Mpemba effect in granular fluids, *Phys. Rev. Lett.* **119**, 148001 (2017).
- [40] A. Torrente, M. A. López-Castaño, A. Lasanta, F. Vega Reyes, A. Prados, and A. Santos, Large Mpemba-like effect in a gas of inelastic rough hard spheres, *Phys. Rev. E* **99**, 060901(R) (2019).
- [41] A. Biswas, V. V. Prasad, O. Raz, and R. Rajesh, Mpemba effect in driven granular Maxwell gases, *Phys. Rev. E* **102**, 012906 (2020).
- [42] E. Mompó, M. A. López-Castaño, A. Torrente, F. Vega Reyes, and A. Lasanta, Memory effects in a gas of viscoelastic particles, *Phys. Fluids* **33**, 062005 (2021).
- [43] R. Gómez González and V. Garzó, Time-dependent homogeneous states of binary granular suspensions, *Phys. Fluids* **33**, 093315 (2021).
- [44] A. Biswas, V. V. Prasad, and R. Rajesh, Mpemba effect in an anisotropically driven granular gas, *EPL* **136**, 46001 (2021).
- [45] A. Biswas, V. V. Prasad, and R. Rajesh, Mpemba effect in anisotropically driven inelastic Maxwell gases, *J. Stat. Phys.* **186**, 45 (2022).
- [46] S. Takada, H. Hayakawa, and A. Santos, Mpemba effect in inertial suspensions, *Phys. Rev. E* **103**, 032901 (2021).
- [47] S. Takada, Homogeneous cooling and heating states of dilute soft-core gases under nonlinear drag, *EPJ Web Conf.* **249**, 04001 (2021).
- [48] M. Baity-Jesi, E. Calore, A. Cruz, L. A. Fernandez, J. M. Gil-Narvión, A. Gordillo-Guerrero, D. Iñiguez, A. Lasanta, A. Maiorano, E. Marinari, V. Martin-Mayor, J. Moreno-Gordo, A. Muñoz-Sudupe, D. Navarro, G. Parisi, S. Perez-Gaviro, F. Ricci-Tersenghi, J. J. Ruiz-Lorenzo, S. F. Schifano, B. Seoane, A. Tarancón, R. Tripicciono, and D. Yllanes, The Mpemba effect in spin glasses is a persistent memory effect, *Proc. Natl. Acad. Sci. U.S.A.* **116**, 15350 (2019).
- [49] P. A. Greaney, G. Lani, G. Cicero, and J. C. Grossman, Mpemba-like behavior in carbon nanotube resonators, *Metall. Mater. Trans. A* **42**, 3907 (2011).
- [50] Y.-H. Ahn, H. Kang, D.-Y. Koh, and H. Lee, Experimental verifications of Mpemba-like behaviors of clathrate hydrates, *Korean J. Chem. Eng.* **33**, 1903 (2016).
- [51] Z. Lu and O. Raz, Nonequilibrium thermodynamics of the Markovian Mpemba effect and its inverse, *Proc. Natl. Acad. Sci. U.S.A.* **114**, 5083 (2017).
- [52] I. Klich, O. Raz, O. Hirschberg, and M. Vucelja, Mpemba index and anomalous relaxation, *Phys. Rev. X* **9**, 021060 (2019).
- [53] R. Chétrite, A. Kumar, and J. Bechhoefer, The metastable Mpemba effect corresponds to a non-monotonic temperature dependence of extractable work, *Front. Phys.* **9**, 654271 (2021).
- [54] D. M. Busiello, D. Gupta, and A. Maritan, Inducing and optimizing Markovian Mpemba effect with stochastic reset, *New J. Phys.* **23**, 103012 (2021).
- [55] J. Lin, K. Li, J. He, J. Ren, and J. Wang, Power statistics of Otto heat engines with the Mpemba effect, *Phys. Rev. E* **105**, 014104 (2022).
- [56] F. J. Schwarzendahl and H. Löwen, Anomalous cooling and overcooling of active systems, [arXiv:2111.06109](https://arxiv.org/abs/2111.06109) 10.48550/arXiv.2111.06109 (2021).
- [57] I. González-Adalid Pemartín, E. Mompó, A. Lasanta, V. Martín-Mayor, and J. Salas, Slow growth of magnetic domains helps fast evolution routes for out-of-equilibrium dynamics, *Phys. Rev. E* **104**, 044114 (2021).
- [58] G. Teza, R. Yaacoby, and O. Raz, Relaxation shortcuts through boundary coupling, [arXiv:2112.10187](https://arxiv.org/abs/2112.10187) 10.48550/arXiv.2112.10187 (2021).
- [59] N. Vadakkayila and S. K. Das, Should a hotter paramagnet transform quicker to a ferromag-

- net? Monte Carlo simulation results for Ising model, *Phys. Chem. Chem. Phys.* **23**, 11186 (2021).
- [60] Z.-Y. Yang and J.-X. Hou, Non-Markovian Mpemba effect in mean-field systems, *Phys. Rev. E* **101**, 052106 (2020).
- [61] Z.-Y. Yang and J.-X. Hou, Mpemba effect of a mean-field system: The phase transition time, *Phys. Rev. E* **105**, 014119 (2022).
- [62] F. Carollo, A. Lasanta, and I. Lesanovsky, Exponentially accelerated approach to stationarity in Markovian open quantum systems through the Mpemba effect, *Phys. Rev. Lett.* **127**, 060401 (2021).
- [63] R. Holtzman and O. Raz, Landau theory for the Mpemba effect through phase transitions, arXiv:2204.03995 10.48550/arXiv.2204.03995 (2022).
- [64] A. Kumar and J. Bechhoefer, Exponentially faster cooling in a colloidal system, *Nature (Lond.)* **584**, 64 (2020).
- [65] A. Kumar, R. Chétrite, and J. Bechhoefer, Anomalous heating in a colloidal system, *Proc. Natl. Acad. Sci. U.S.A.* **119**, e2118484119 (2022).
- [66] S. Kullback and R. A. Leibler, On information and sufficiency, *Ann. Math. Statist.* **22**, 79 (1951).
- [67] N. G. V. Kampen, *Stochastic Processes in Physics and Chemistry* (North-Holland, Amsterdam, 2007).
- [68] Strictly speaking, the KLD does not have the properties of a distance; e.g., it does not satisfy the triangle inequality.
- [69] G. W. Scherer, Theories of relaxation, *J. Non-Cryst. Solids* **123**, 75 (1990).
- [70] A. Cavagna, Supercooled liquids for pedestrians, *Phys. Rep.* **476**, 51 (2009).
- [71] L. Berthier and G. Biroli, Theoretical perspective on the glass transition and amorphous materials, *Rev. Mod. Phys.* **83**, 587 (2011).
- [72] J. J. Brey and A. Prados, Dynamical behavior of a one-dimensional Ising model submitted to continuous heating and cooling processes, *Phys. Rev. B* **49**, 984 (1994).
- [73] L. Ferrari, Particles dispersed in a dilute gas: Limits of validity of the Langevin equation, *Chem. Phys.* **336**, 27 (2007).
- [74] L. Ferrari, Particles dispersed in a dilute gas. II. From the Langevin equation to a more general kinetic approach, *Chem. Phys.* **428**, 144 (2014).
- [75] M. Hohmann, F. Kindermann, T. Lausch, D. Mayer, F. Schmidt, E. Lutz, and A. Widera, Individual tracer atoms in an ultracold dilute gas, *Phys. Rev. Lett.* **118**, 263401 (2017).
- [76] J. R. Dorfman and H. van Beijeren, The kinetic theory of gases, in *Statistical Mechanics, Part B*, edited by B. Berne (Plenum, New York, 1977) pp. 65–179.
- [77] Note that, because of the second equality in Eq. (12b), the entropic “distance” \mathcal{D} from f to f^{eq} is exactly given by the distance from f to f^{LE} plus the distance from f^{LE} to f^{eq} . The decomposition (11) can be schematically depicted as
- $$\overbrace{f(\mathbf{v}, t) \longrightarrow f^{\text{LE}}(\mathbf{v}; T(t)) \longrightarrow f^{\text{eq}}(\mathbf{v})}^{\mathcal{D}(t)}.$$
- $\underbrace{\hspace{1.5cm}}_{\mathcal{D}^{\text{kin}}(t)} \qquad \underbrace{\hspace{1.5cm}}_{\mathcal{D}^{\text{LE}}(T(t))}$
- [78] The sketch in Fig. 2 was actually obtained from the solution of the BSA (see Sec. B 1) and the application of Eqs. (12b) and (23) for the initial condition $\theta^0 = 2$, $a_2^0 = 0.5$.
- [79] T. R. Kirkpatrick, D. Belitz, and J. R. Dorfman, Non-hydrodynamic initial conditions are not soon forgotten, *Phys. Rev. E* **104**, 024111 (2021).
- [80] In that case, $\tau_b \rightarrow \infty$ and one has to change the definition of dimensionless time to $\zeta_0 t$.
- [81] M. Jauregui, A. L. F. Lucchi, J. H. Y. Passos, and R. S. Mendes, Stationary solution and \hbar theorem for a generalized Fokker-Planck equation, *Phys. Rev. E* **104**, 034130 (2021).
- [82] This was the approach carried out in a previous work to analyze the TME [36].
- [83] This approximation has been employed in Ref. [37] to study the response of the nonlinear fluid to a low-temperature quench.
- [84] For the EME, there is not a clear cut distinction between the direct and inverse EME (since the relative entropy \mathcal{D} is positive definite), unless the initial temperatures are known.
- [85] R. V. Hogg and A. T. Craig, *Introduction to Mathematical Statistics*, 4th ed. (Macmillan Publishing, New York, 1978) pp. 103–108.
- [86] W. D. Penny, KL-Divergences of Normal, Gamma, Dirichlet, and Wishart densities, www.fil.ion.ucl.ac.uk/~wpenny/publications/densities.ps.
- [87] M. Abramowitz and I. A. Stegun, eds., *Handbook of Mathematical Functions* (Dover, New York, 1972).
- [88] A. J. Kovacs, Transition vitreuse dans les polymères amorphes. Etude phénoménologique, *Fortschr. Hochpolym.-Forsch.* **3**, 394 (1963).
- [89] A. J. Kovacs, J. J. Aklonis, J. M. Hutchinson, and A. R. Ramos, Isobaric volume and enthalpy recovery of glasses. II. A transparent multiparameter theory, *J. Polym. Sci. Polym. Phys. Ed.* **17**, 1097 (1979).
- [90] A. Prados and J. J. Brey, The Kovacs effect: a master equation analysis, *J. Stat. Mech.*, P02009 (2010).
- [91] E. Bouchbinder and J. S. Langer, Nonequilibrium thermodynamics of the Kovacs effect, *Soft Matter* **6**, 3065 (2010).
- [92] A. Prados and E. Trizac, Kovacs-like memory effect in driven granular gases, *Phys. Rev. Lett.* **112**, 198001 (2014).
- [93] E. Trizac and A. Prados, Memory effect in uniformly heated granular gases, *Phys. Rev. E* **90**, 012204 (2014).
- [94] A. Lasanta, F. Vega Reyes, A. Prados, and A. Santos, On the emergence of large and complex memory effects in nonequilibrium fluids, *New J. Phys.* **21**, 033042 (2019).
- [95] A. Megias and A. Santos, Kullback–Leibler divergence of a freely cooling granular gas, *Entropy* **22**, 1308 (2020).
- [96] A. Megias and A. Santos, Relative entropy of freely cooling granular gases. A molecular dynamics study, *EPJ Web Conf.* **249**, 04006 (2021).
- [97] A similar distance to a local equilibrium distribution has been recently introduced to analyze the relaxation of an Ising ferromagnet in the weak coupling limit [108].
- [98] A. Lapolla and A. Godec, Faster uphill relaxation in thermodynamically equidistant temperature quenches, *Phys. Rev. Lett.* **125**, 110602 (2020).
- [99] T. Van Vu and Y. Hasegawa, Toward relaxation asymmetry: Heating is faster than cooling, *Phys. Rev. Res.* **3**, 043160 (2021).

- [100] R. Mannella and P. V. E. McClintock, Itô versus Stratonovich: 30 years later, *Fluct. Noise Lett.* **11**, 1240010 (2012).
- [101] Y. L. Klimontovich, Nonlinear Brownian motion, *Physics-Uspekhi* **37**, 737 (1994).
- [102] N. Brilliantov and T. Pöschel, Breakdown of the Sonine expansion for the velocity distribution of granular gases, *Europhys. Lett.* **74**, 424 (2006), Erratum: **75**, 188 (2006).
- [103] G. A. Bird, *Molecular Gas Dynamics and the Direct Simulation of Gas Flows* (Clarendon, Oxford, UK, 1994).
- [104] G. A. Bird, *The DSMC Method* (CreateSpace Independent Publishing Platform, Scotts Valley, CA, 2013).
- [105] J. M. Montanero and A. Santos, Computer simulation of uniformly heated granular fluids, *Granul. Matter* **2**, 53 (2000).
- [106] A. Scala, Event-driven Langevin simulations of hard spheres, *Phys. Rev. E* **86**, 026709 (2012).
- [107] A. Santos and J. M. Montanero, The second and third Sonine coefficients of a freely cooling granular gas revisited, *Granul. Matter* **11**, 157 (2009).
- [108] G. Teza, R. Yaacoby, and O. Raz, Far from equilibrium relaxation in the weak coupling limit, arXiv:2203.11644 10.48550/arXiv.2203.11644 (2022).